AFOSR-TR-97 0649

# REPORT DOCUMENTATION PAGE

Form Approved
OMB No. 0704-0188



| 1. AGENCY USE ONLY (Leave blank) | 2. REPORT DATE | 3. REPORT TYPE AND DATES COVERED |
|---|---|---|
| | October 6, 1997 | Final Report (25 May 1994 – 24 May 1997) |

**4. TITLE AND SUBTITLE**

Investigation of Characteristics of Seismic Waves from the May 21, 1992 Lop Nor Nuclear Explosion Using IRIS Broadband Data

**5. FUNDING NUMBERS**

F49620-94-1-0315

**6. AUTHOR(S)**

Jiajun Zhang

**7. PERFORMING ORGANIZATION NAME(S) AND ADDRESS(ES)**

University of California, Santa Cruz
Institute of Tectonics
Santa Cruz, CA 95064

**8. PERFORMING ORGANIZATION REPORT NUMBER**

**9. SPONSORING/MONITORING AGENCY NAME(S) AND ADDRESS(ES)**

AFOSR/NL (Sponsor)
110 Duncan Ave, Suite B115
Bolling AFB, DC 20332-8050
Prof. Man.: Stanley Dickinson/NL

**10. SPONSORING/MONITORING AGENCY REPORT NUMBER**

**11. SUPPLEMENTARY NOTES**



**12a. DISTRIBUTION/AVAILABILITY STATEMENT**

Approval for public release: distribution unlimited

**12b. DISTRIBUTION CODE**

**13. ABSTRACT** *(Maximum 200 words)*

This is the final report for this grant to develop new seismological techniques for source characterization of nuclear explosions and earthquakes using broadband waveforms. Two studies are presented. The first study demonstrated that source parameters determined using routine methods are often biased due to unmodeled effects of the Earth's structure. For the January 17, 1994 Northridge, California earthquake, we examined the results obtained using various techniques and concluded that a special technique must be developed for characterization of seismic events when the Earth's velocity and attenuation structure is only moderately constrained. The primary effects of the study were directed at developing a new approach to optimizing the performance of source inversion methods. The efforts resulted in the development of an algorithm called the Earth Simplifying Transformation (EST), which can be incorporated in various methods of waveform analysis for improved source characterization. The second study extended and applied the EST algorithm to the broadband seismic recordings from earthquakes and nuclear explosions in Xinjiang, China. These studies demonstrated that the EST method holds promise for reliable source characterization for small events in a calibrated region and that the primary use of the method is in improving empirical calibrations in seismic-event monitoring.

**14. SUBJECT TERMS**

Seismic Source
Nuclear Explosions



**15. NUMBER OF PAGES**

28

**16. PRICE CODE**

| 17. SECURITY CLASSIFICATION OF REPORT | 18. SECURITY CLASSIFICATION OF THIS PAGE | 19. SECURITY CLASSIFICATION OF ABSTRACT | 20. LIMITATI |
|---|---|---|---|
| Unclassified | Unclassified | Unclassified | SAR |

# Table of Contents

JOURNAL OF GEOPHYSICAL RESEARCH, VOL. 102, NO. B4, PAGES 8159–8169, APRIL 10, 1997

# Determination of earthquake source mechanisms using teleseismic 30-140 s waves: The January 17, 1994, Northridge earthquake

Jiajun Zhang,[1] Keiko Kuge,[2] Thorne Lay,[1] and Seiji Tsuboi[3]

**Abstract.** Complete seismic waveforms with periods between 30 and 140 s recorded at teleseismic distances (≥ 10°) are used to determine the source mechanism of the January 17, 1994, Northridge earthquake ($M_s$ = 6.8). An algorithm called the Earth simplifying transformation (EST) is applied to the mainshock (primary event) data to calibrate and remove propagation effects of Earth's lateral and radial heterogeneities that are not predicted by a reference Earth model. The procedure involves frequency domain division of each pair of observed and synthetic waveforms for an auxiliary event with a well-constrained source mechanism in proximity to the primary event, with the synthetics being computed for a reference Earth model. If the auxiliary event source mechanism is correct, the differences between the data and synthetics represent the residual effects of the Earth's structure that are not predicted by the Earth model. The frequency dependent deconvolution filters are convolved with the corresponding observed signals for the primary event. The resulting waveforms are then used to determine the source mechanism of the primary event by forward modeling and by centroid-moment-tensor inversion, with excellent fits to the complete waveforms being achieved. The resulting solution for the Northridge event has a centroid depth of 12±1 km and a mechanism with strike, $\phi$ = 115°, dip, $\delta$ = 40°, and rake, $\lambda$ = 95°, with 5° uncertainty for each parameter. The EST procedure holds promise for reliable source inversion for small earthquakes in a region calibrated by large events with well-determined source parameters.

## Introduction

The January 17, 1994, Northridge ($M_s$ = 6.8) earthquake ruptured a south dipping fault beneath the San Fernando Valley in the Los Angeles region [e.g., *Hauksson et al.*, 1995]. This was the most damaging large earthquake in the region, which has suffered an increased level of seismicity in the past decade. Recent progress in the worldwide deployment of broadband seismic stations allows the seismic radiation from earthquakes in southern California to be analyzed with unprecedented azimuthal coverage. For the assessment of regional seismic hazards, source mechanisms of large earthquakes in this region are routinely determined using various data sets, typically including *P* wave first motions, and body and surface waves recorded at local, regional, and teleseismic distances [e.g., *Bent and Helmberger*, 1989; *Bent et al.*, 1989; *Kanamori et al.*, 1990; *Wald et al.*, 1990; *Patton and Zandt*, 1991; *Romanowicz et al.*, 1992, 1993, 1994; *Kanamori et al.*, 1992; *Uhrhammer*, 1992; *Uhrhammer et al.*, 1994; *Zhao and Helmberger*, 1994; *Dreger*, 1994; *Ritsema and Lay*, 1995; *Thio and Kanamori*, 1995; *Pasyanos et al.*, 1996].

Table 1 lists hypocentral parameters of the Northridge earthquake (hereinafter referred to as event I) along with focal mechanisms obtained previously using three methods: *P* wave first motions, regional waveform inversion, and routine centroid-moment-tensor (CMT) inversion, which are referred to as PFM, RWI and CMT mechanisms, respectively. The regional waveform solution obtained by *Dreger* [1994] is referred to as RWI1 and that by *Song et al.* [1995] to as RWI2. Figure 1 shows that there are moderate differences between these estimated source mechanisms for the Northridge earthquake. Precise determination of the rupture geometry and slip distribution requires high precision in the point-source model [e.g., *Wald et al.*, 1996], so it is important to resolve which model is optimal and to reduce model errors which may bias the solutions.

Table 1 also lists mechanisms for two nearby events: an aftershock ($M_s$ = 6.0) of the Northridge event, and the June 28, 1991, Sierra Madre earthquake ($M_s$ = 5.2) (hereinafter referred to as events II and III, respectively). Events II and III are located 19 km N50°W and 50 km N84°E from event I, respectively. In the regional waveform inversions, the data for event III included $P_{nl}$ and $S_n$ waves, while for events I and II both body and surface waves (with periods 20-100 s) were used. In the CMT inversions, the data used for events II and III are long-period body waves, while the data for event I include surface waves with periods longer than 135 s and long-period body waves.

The source mechanisms for each event listed in Table 1 differ mainly in dip angle and strike direction. For the south dipping nodal planes, the dip angle ranges from 35° to 53°, 43° to 45°, and 41° to 43° for events I, II, and III, respectively; and the strike ranges from 105° to 130°, 100° to 116°, and

[1] Institute of Tectonics and W. M. Keck Seismological Laboratory, University of California, Santa Cruz.
[2] Department of Geophysics, Kyoto University, Kyoto, Japan.
[3] Department of Geoscience, National Defense Academy, Yokosuka, Japan.



Paper number 96JB03913.
0148-0227/97/96JB-03913$09.00

**Table 1.** Source Parameters of Earthquakes Used in This Study

| | Event I Northridge (Mainshock) | Event II Northridge (Aftershock) | Event III Sierra Madre |
|---|---|---|---|
| Origin Time, UTC | Jan. 17, 1994, 1230:55.4 | Jan. 17, 1994, 2333:30.7 | June 28, 1991, 1443:54.5 |
| Location | 34.213°N, 118.536°W | 34.326°N, 118.698°W | 34.26°N, 118.00°W |
| Depth, km | 18.2 | 9.8 | 12.0 |
| $M_s$ | 6.8 | 6.0 | 5.2 |
| | *First Motion Solution* | | |
| Strike/dip/slip[a] | 105/35/100; 273/56/83 | 100/45/70; 307/48/109 | 242/50/82; 74/41/99 |
| | *Regional Wave Solution* | | |
| Strike/dip/slip[b] | 121/43/105; 280/49/76 | 116/43/92; 294/47/88 | 235/50/74; 79/43/108 |
| Strike/dip/slip[c] | 128/33/106; 289/58/80 | | |
| | *CMT Solution*[d] | | |
| Location | 34.44°N, 118.64°W | 34.22°N, 118.70°W | 34.26°N, 118.00°W |
| Depth, km | 16.8 | 15.0 | 20.9 |
| Centroid time, s | 8.2 | 4.9 | 5.5 |
| Half duration | 5.4 | 1.9 | 2.6 |
| Best double couple mechanism | 130/53/111; 278/42/65 | 115/45/89; 296/45/91 | 223/58/58; 93/43/130 |
| $M_0$ | $1.2\times 10^{19}$ N m | $7.0\times 10^{17}$ N m | $3.5\times 10^{17}$ N m |
| $M_w$ | 6.7 | 5.8 | 5.6 |

The origin time, hypocentral location and depth, and $M_s$ are from the Southern California Seismographic Network operated by California Institute of Technology and U.S. Geological Survey.

[a] *Hauksson* [1994, also personal communication, 1994]; *Hauksson et al.* [1995].

[b] *Dreger and Helmberger* [1991]; *Dreger* [1994, also personal communication, 1994].

[c] *Song et al.* [1995].

[d] *Dziewonski et al.* [1992, 1994].

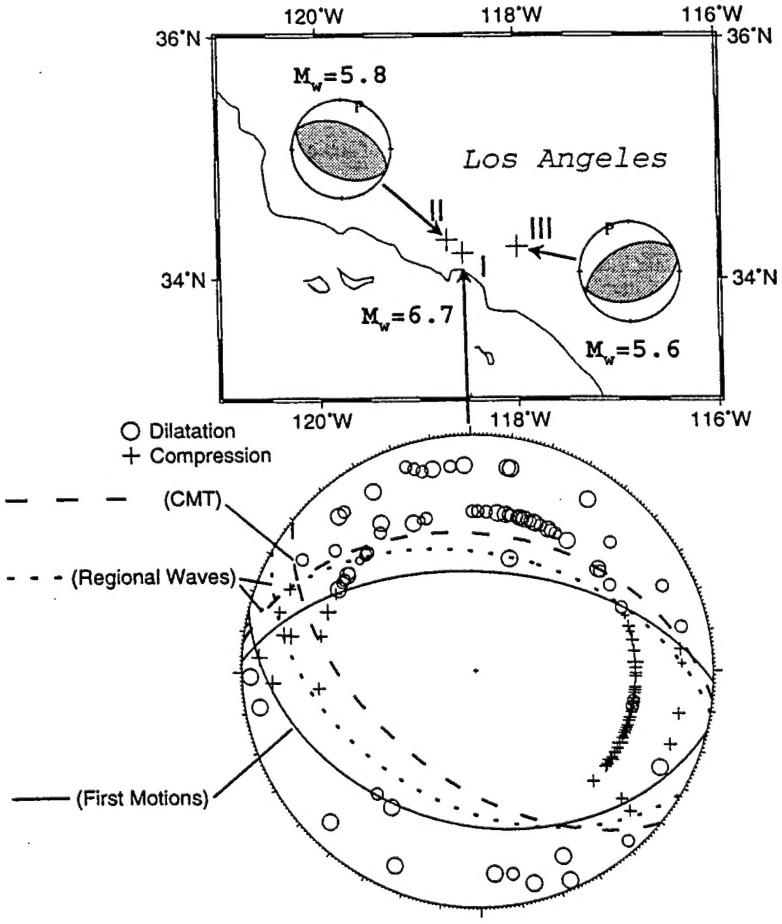


**Figure 1.** Epicentral location (pluses) and source mechanisms of the 1994 Northridge (I, mainshock; II, aftershock) and 1991 Sierra Madre (III) earthquakes (Table 1). The mechanism for event II is the solution from regional wave inversions [*Dreger*, 1994], and for event III the solution is from *P* wave first motions. First motion data for the Northridge mainshock were obtained by *Hauksson et al.* [1995] and are shown below in an equal-area projection with the confidence level indicated by the size of each symbol. Three focal mechanism solutions listed in Table 1 are also shown (regional wave solution is from *Dreger* [1994]).

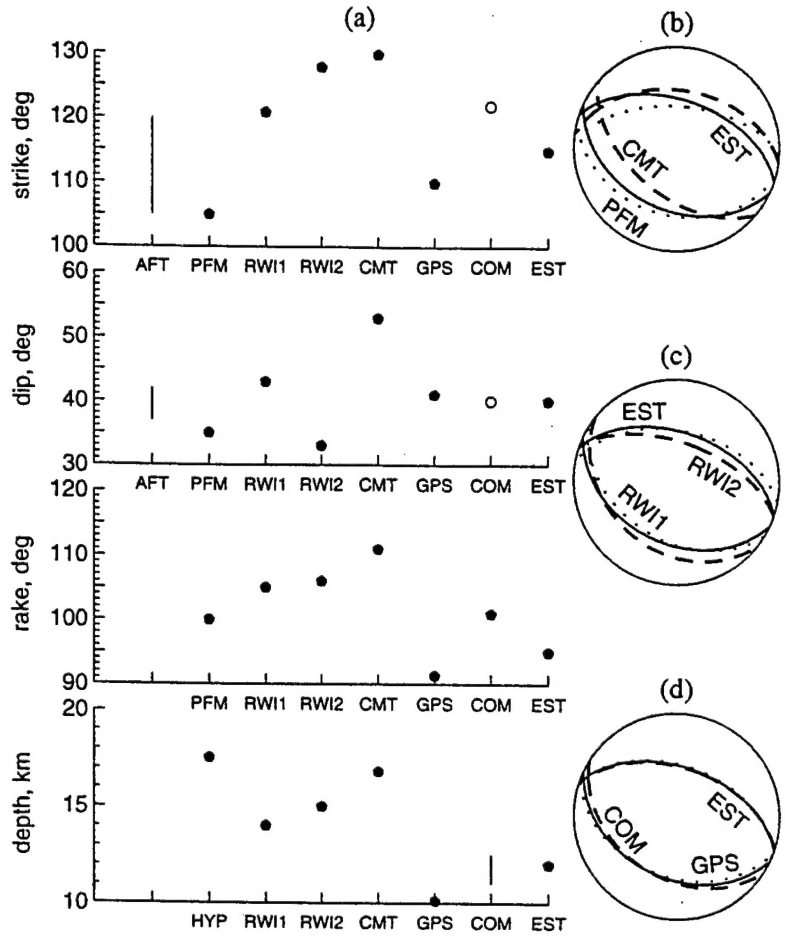


**Figure 2.** (a) Summary of focal mechanism and centroid depth estimates for the Northridge mainshock obtained from various studies. AFT, aftershock distribution [*Hauksson et al.*, 1995]; PFM, *P* wave first motions [*Hauksson et al.*, 1995]; regional waveform inversions (RWI1 [*Dreger*, 1994]; RWI2 [*Song et al.*, 1995]); CMT, Harvard CMT solution; GPS, GPS observations [*Hudnut et al.*, 1996]; COM, combined dislocation model (open circle indicating parameters constrained from aftershock distributions) [*Wald et al.*, 1996]; EST, this study; HYP, hypocentral depth [*Wald et al.*, 1996]. Bars indicate ranges of possible estimates. (b-d) Comparisons of the EST solution (solid lines) with the source models (dotted and dashed lines) of PFM and CMT (Figure 2b), RWI1 and RWI2 (Figure 2c), and GPS and COM (Figure 2d).

73° to 93° for events I, II, and III, respectively. Note the common tendency for the strike direction in the CMT mechanisms to be rotated clockwise by 15° to 25° relative to the PFM mechanisms. The estimated uncertainties of the dip and strike angles for PFM and RWI1 mechanisms are in general less than 5° (E. Hauksson and D. Dreger, personal communication, 1994). This is small in comparison with the variations in estimated mechanisms.

For the Northridge mainshock, the differences between point-source mechanism estimates obtained from various methods (Figure 2) may be attributed to uncertainties or biases in these estimates, which must be identified and reduced when possible, or attributed to mechanism changes in the rupture process. *Hauksson et al.* [1995] pointed out that there is an increase in dip along strike in the distribution of aftershocks, and they attributed the difference between the mainshock mechanisms obtained from various methods to a curved rupture surface. However, comparable differences between the estimated source mechanisms are also found for relatively small events in this region, such as events II and III (Table 1), which suggests that the inconsistency may instead reflect model errors associated with the different methods. Systematic mechanism inconsistencies are often found in the Preliminary Determination of Epicenters Monthly Listings for earthquakes in southern California, in particular, for events with large magnitude ($M_s \geq 6.5$). Usually, the formal uncertainty of the mechanism for each method is much smaller than the differences between the mechanisms, reflecting the fact that the formal uncertainties do not take into account model uncertainties.

In addition to differences between source mechanism estimates for the Northridge mainshock, there are also moderate differences between the centroid depth estimates obtained in various studies. *Thio and Kanamori* [1996] obtained a source model from inversions of teleseismic body wave data, which consists of three subevents located at depths of 19, 17.5, and 14 km with more than 75% of the seismic moment being released by the two deeper subevents. This is consistent with the CMT depth of 16.8 km. Studies of strong motions by *Wald and Heaton* [1994] and regional waveforms by *Dreger* [1994] also favor slip occurring at large depths. However, analyses of geodetic data by *Hudnut et al.* [1996] and *Shen et al.* [1996] prefer a shallower centroid depth (about 10 km).

**Table 2.** Comparison of Source Models for the Northridge Mainshock

| Method | Centroid Depth, km | Strike | Dip | Rake | Moment, $10^{19}$ N m |
|---|---|---|---|---|---|
| COM | 11-12.5 | 122° [a] | 40° [a] | 101° | 1.4 |
| GPS | 10.1 | 110° | 41° | 91° | 1.1 |
| EST | 12 | 115° | 40° | 95° | 1.2 [b] |

COM, *Wald et al.* [1996]; GPS, *Hudnut et al.* [1996]; EST, this study.
[a] Inferred from aftershock distributions.
[b] Moment-tensor solution has a nondouble couple component less than 1%.

The combined model for displacement time histories obtained by *Wald et al.* [1996] from joint inversion of strong-motion, teleseismic, Global Positioning System (GPS), and leveling data shows that large displacements were concentrated at shallow depths updip from the hypocenter. Using this model, we estimated the centroid depth at between 11 and 12.5 km (Table 2 and Figure 2), which is slightly deeper than the 10 km centroid depth obtained from the geodetic data analysis. This difference may be attributed to the difficulty of recovering slip near the downdip edge of the rupture plane with the available GPS data [*Hudnut et al.*, 1996]. However, it remains to be seen whether the resolving power of teleseismic data can be improved to allow us to obtain a shallow centroid depth consistent with that for combined seismological and geodetic data.

We previously performed a CMT-type analysis of the source mechanism of the Northridge earthquake, in which we used the laterally homogeneous preliminary reference Earth model (PREM) [*Dziewonski and Anderson*, 1981], and found strong data dependence of the solution [*Zhang et al.*, 1994]. For many stations, the observed data differ significantly from the model predictions. In order to reduce the biases due to unmodeled effects of Earth's structure, we incorporated recently developed three-dimensional models of the Earth in our long-period surface wave CMT inversions, basically replicating the procedure currently used at Harvard. The aspherical Earth model corrections did not reduce the discrepancies to a significant extent. We infer that even for long-period (> 135 s) surface waves the existing aspherical models cannot eliminate all actual propagation effects, and this certainly holds for the shorter period signals.

In this study we use 30 to 140 s surface waves recorded at teleseismic distances to further constrain the source mechanism of the 1994 Northridge earthquake. Our data set consists of Global Seismographic Network seismic waves recorded at epicentral distances larger than 10° for the 1994 Northridge mainshock and two events near the mainshock epicenter (Figure 1). The data are dominated by high signal-to-noise ratio surface waves, which must be accurately corrected for propagation effects. At present this can only be done empirically. Our objectives are to exploit the neglected surface wave information to refine the Northridge source mechanism and to develop a general strategy for including this energy in systematic inversions for smaller events in a calibrated region.

The procedure followed consists of the following steps. First, we compute synthetics for a reference Earth model using an a priori, well-constrained focal mechanism for a nearby auxiliary event. By deconvolving the synthetic signals from data for the auxiliary event, we obtain complex transfer functions or deconvolution filters that represent the propagation effects which are not predicted by the Earth model. This is equivalent to complete waveform calibration of wave propagation effects for each path to optimize the performance of source inversion methods. By removing the empirically determined propagation effects relative to a known model from the observed waveforms for the Northridge mainshock (primary event), we obtain simplified waveforms, which are intrinsically well modeled by the reference Earth model. These waveforms are then compared with the synthetics for the reference Earth model using several source mechanism solutions obtained previously for the Northridge mainshock, along with waveform inversion of the complete signals. The excellent fit to the waveforms that is obtained indicates the general utility of this method for high-precision focal mechanism determination. This approach constitutes a complete waveform generalization of empirical path correction methods such as those of *Weidner and Aki* [1973] and *Patton* [1980].

## Method

Following *Gilbert and Dziewonski* [1975], the spectrum of a component of ground motion excited by a point source at angular frequency $\omega$ for a reference Earth model may be given by

$$u_k(\mathbf{x}, \omega) = \sum_{i=1}^{6} \psi_{ki}(\mathbf{x}, \mathbf{x}_s, \omega) f_i(\omega) \tag{1}$$

where $u_k$ is the $k$th record in a set of seismograms, with the receiver at position $\mathbf{x}$ and the source at $\mathbf{x}_s$; $\psi_{ki}$ are excitation kernels, and the $f_i$ represents six independent components of the moment-rate tensor. For another event located at $\mathbf{x}_s'$ with moment-rate tensor $f_i'$, the spectrum may be given by

$$u_k'(\mathbf{x}, \omega) = \sum_{i=1}^{6} \psi_{ki}(\mathbf{x}, \mathbf{x}_s', \omega) f_i'(\omega). \tag{2}$$

Taking into account our imperfect knowledge of Earth structure and background noise, the spectra of observed ground motion for these events may be expressed as

$$U_k(\mathbf{x}, \omega) = u_k(\mathbf{x}, \omega)\, \alpha_k(\mathbf{x}, \omega) + \varepsilon(\mathbf{x}, \omega) \tag{3a}$$

$$U_k'(\mathbf{x}, \omega) = u_k'(\mathbf{x}, \omega)\, \alpha_k'(\mathbf{x}, \omega) + \varepsilon'(\mathbf{x}, \omega) \tag{3b}$$

where $\alpha$ and $\alpha'$ represent effects of the deviation of the Earth's structure from the Earth model, assuming that source parameters are perfectly known. In the following analysis the noise terms ($\varepsilon$ and $\varepsilon'$) are ignored and the event at $\mathbf{x}_s$ is referred to as the primary event, while the event at $\mathbf{x}_s'$ is an auxiliary event. In conventional algorithms, the moment-rate tensor of the primary event, $f_i$, is determined from data for the event, $U_k$, by solving the following equation

$$U_k(\mathbf{x}, \omega) = \sum_{i=1}^{6} \psi_{ki}(\mathbf{x}, \mathbf{x}_s, \omega)\, f_i(\omega), \quad (4)$$

which is correct to zeroth order in terms of $\alpha$, since implicit in the algorithms is the assumption

$$\alpha_k(\mathbf{x}, \omega) = 1. \quad (5)$$

The question that we shall address in this study is as follows. Given a set of seismograms, $U_k$ and $U_k'$, at common stations from two events, which are located in proximity (in comparison with the event station distance), along with synthetics for the auxiliary event, $u_k'$, computed for a given (correct) focal mechanism and Earth model, is it possible to determine the moment-rate tensor of the primary event, $f_i$? For this purpose we define the following transformation

$$u_P^A(\mathbf{x}, \omega) = u_k'(\mathbf{x}, \omega)\, U_k(\mathbf{x}, \omega) \,/\, U_k'(\mathbf{x}, \omega), \quad (6)$$

which is referred to as the Earth simplifying transformation (EST) in the following analysis. If there is good correlation between the data for the primary and auxiliary events despite their differences in polarity and instantaneous phase for various wave packets, we may assume

$$\alpha_k(\mathbf{x}, \omega) = \alpha_k'(\mathbf{x}, \omega). \quad (7)$$

In this study, our data sets for various events listed in Table 1 show good correlations, and the excellent fit to the simplified signals that is obtained indicates the reliability of this assumption. The accuracy of this assumption is influenced by the proximity of the events and the frequency content of the data. Given multiple auxiliary events in a region, one could average deconvolution filters or spatially interpolate them to strengthen this approximation, and to reduce error due to incorrect auxiliary event source parameters. Assuming (7), the right-hand side of (6) becomes $u_k(\mathbf{x}, \omega)$, thus the spectrum of the EST waveform may be expressed as

$$u_P^A(\mathbf{x}, \omega) = \sum_{i=1}^{6} \psi_{ki}(\mathbf{x}, \mathbf{x}_s, \omega)\, f_i(\omega) \quad (8)$$

which is correct to first order in terms of $\alpha$ and will be used to determine the moment-rate tensor ($f_i$). For simplicity of analysis, we adopt a frequently used assumption: the $f_i$ are considered to be independent of frequency except for a common correction for an assumed duration of the source and are regarded as the moment tensor.

In this study, various experiments were made to explore the sensitivity of primary event source parameters obtained from inversions of EST waveforms to the prescribed source parameters of the auxiliary event. Clearly, errors in auxiliary event centroid estimates (time, location, and depth) will project into the primary event solution, influencing not only centroid but also source mechanism estimates, so good independent constraints on the auxiliary event centroid parameters are critical. However, an interesting and important question is how errors in the auxiliary event source mechanism project into the primary event solution.

To address this question, we use an arbitrarily given moment tensor $g_i'$ in the calculation of synthetics for the auxiliary event. If $f_i'$ is the true moment tensor of the auxiliary event, the errors in the auxiliary event source mechanism are $g_i'-f_i'$. The errors can be also described by the linear relation: $g_i' = f_i'\, d_i$, $(i = 1, ..., 6)$. Then the EST waveforms corresponding to the incorrect auxiliary event moment tensor $g_i'$ may be written as

$$u_P^A(\mathbf{x}) = \sum_{i=1}^{6} \psi_{ki}(\mathbf{x}, \mathbf{x}_s)\, g_i, \quad (9)$$

with $g_i = f_i\, d_i$, $(i = 1, ..., 6)$, where $f_i$ is the true moment tensor of the primary event. Clearly, one will recover a biased source mechanism for the primary event, with linear dependence on the auxiliary event solution.

However, since both the EST waveforms in (9) and (8) correspond to the same set of excitation kernels, inversions of biased EST waveforms (9) will yield the same centroid estimates as for correct EST waveforms (8). Therefore, errors in the auxiliary event source mechanism do not project into errors in the primary event centroid estimates. It follows that using well-determined centroid parameters of the auxiliary event, reliable centroid parameters of the primary event can be obtained even by inverting EST waveforms that are computed for an arbitrarily given auxiliary event moment tensor. Our experiments on the Northridge earthquake data set confirm that variation of the prescribed auxiliary event moment tensor does not affect the primary event centroid estimate.

The linear dependence of the derived primary event moment tensor on the prescribed auxiliary event moment tensor allows us to estimate any possible biases in the primary event moment-tensor solution, if the biases in the auxiliary event moment tensor are determined. This is achieved by first estimating bias factors $d_i$ for the prescribed auxiliary event moment tensor and then calculating the resulting errors in the primary event moment-tensor solution: $g_i-g_i/d_i$, $(i = 1, ..., 6)$.

## Application to Teleseismic Surface Waves

In comparison with conventional algorithms, in which the moment tensor of an event is directly determined using data for the event itself, the EST algorithm introduced here requires additional data from the auxiliary event, which must be located at a close distance to the primary event (in comparison with the event station distance) and must have a known moment tensor. Note that the relaxation of the strong assumption (5) involved in conventional algorithms allows us to make use of all seismic waves, in particular surface waves with periods less than about 140 s; these waves are typically so strongly affected by the complexity of the Earth's structure, including both lateral and radial heterogeneities, that direct inversion of the short-period surface waves is not possible.

In this section we first show several EST waveforms obtained for the Northridge mainshock (the primary event) using events II and III as auxiliary events. Note that the focal mechanism of event III (the 1991 Sierra Madre earthquake) is characterized by nodal planes dipping in the NW-SE direction, in clear contrast with the NE-SW dipping directions of nodal planes for the Northridge mainshock (Figure 1). Using two auxiliary events with different locations, depths, and source mechanisms allows us to examine the validity of the assumptions in the proposed algorithm and to explore any biases in the results due to our choice of auxiliary event.

Figure 3 shows displacement waveforms, band-pass filtered between 7 and 30 mHz, recorded at station WMQ from events I and III for vertical and radial components and from events I and II for the transverse component (the transverse component at this station from event III is very noisy and is not shown here, but transverse components for many other stations were used in our analysis.). The station is located at teleseismic distance from the source region, and the waveforms are dominat-

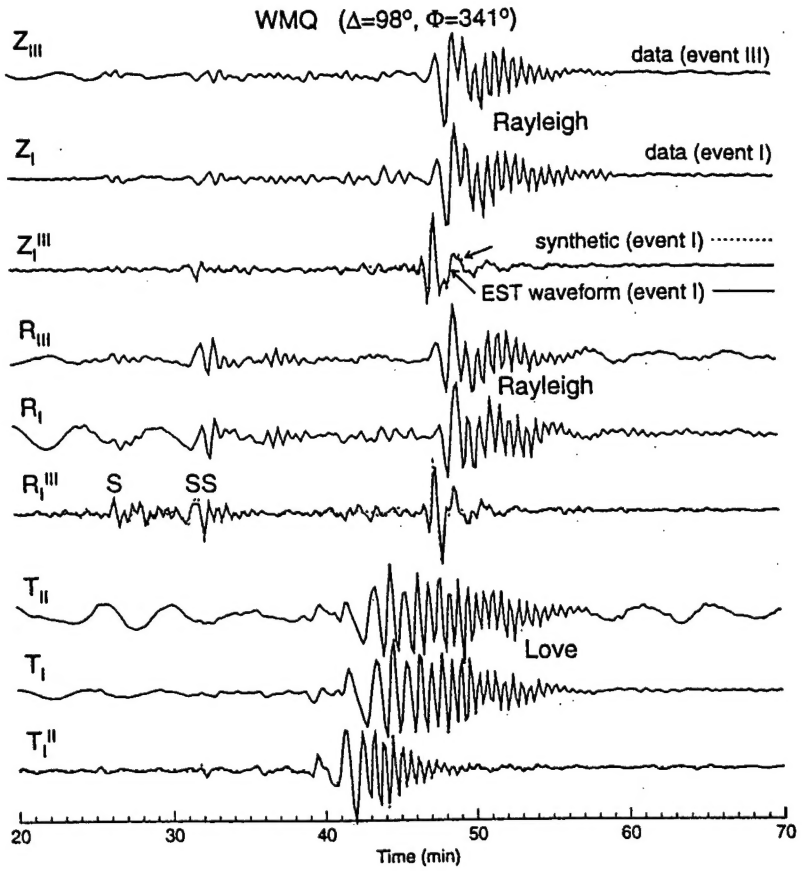


**Figure 3.** Vertical ($Z$), radial ($R$), and transverse ($T$) components of data and synthetics at station WMQ (Urumqi, China). Symbols $Z$, $R$, and $T$ with subscripts ($I$, $II$, and $III$) indicate ground displacements, with the subscript identifying the event listed in Table 1 and shown in Figure 1. Symbols $Z_I^{III}$, $R_I^{III}$, and $T_I^{II}$ indicate EST waveforms for the Northridge mainshock (event I), with the superscript identifying the auxiliary event used. Dotted lines indicate synthetics for the Northridge mainshock computed for the focal mechanism from $P$ wave first motions. Amplitude is arbitrarily set to show waveform coherence. Time is measured from the origin time of the corresponding event.

ed by large-amplitude fundamental mode surface waves. Comparison of the waveforms indicates that for each component there is good coherence between the observed waveforms for the primary and auxiliary events. This indicates that for this station the signals are primarily shaped by the common propagation effects, implying that (7) is a good approximation for paths to this station.

Figure 3 also shows the synthetics computed for Earth model PREM for the Northridge mainshock (primary event) using the PFM mechanism (dotted lines). It is clear that there is considerable discrepancy between the arrival time and dispersion characteristics of the observed waveforms ($Z_I$, $R_I$, and $T_I$) and synthetics for the primary event. Synthetics calculated using other focal mechanisms listed in Table 1 for the Northridge mainshock have waveforms similar to those for the PFM mechanism, but for several stations there are significant differences in amplitudes. The amplitude effects will be discussed later, but it is clear that direct inversion of these signals using the PREM model will fail to resolve the source. For this reason, standard CMT inversions completely filter out all of the surface wave signal seen in Figure 3.

Figure 3 further shows the EST waveforms, with $Z_I^{III}$, $R_I^{III}$, and $T_I^{II}$ (solid lines) corresponding to vertical, radial, and transverse components, respectively, where the superscript indicates the auxiliary event used. In the calculation of the EST waveforms, the synthetics for the auxiliary event are computed for a point source with a step-time function located at the hypocenter with the PFM mechanism used for event III and the RWI1 mechanism used for event II. Note that for $Z_I^{III}$ and $R_I^{III}$, although the mechanism of the auxiliary event (event III) is very different from that of the primary event (Figure 1 and Table 1), the fit of the PREM synthetics to the EST waveforms is excellent, demonstrating the validity of assumption (7).

In the calculation of each EST waveform, the convolution and deconvolution of data and synthetics are performed in the frequency domain, and truncation is used when peaks and holes of the spectra for the two events mismatch, resulting in exceptionally large peaks in the EST spectra. Other common techniques, such as smoothing or filtering, may also be used to reduce the instabilities associated with deconvolution.

Now we compare EST waveforms with the synthetics predicted for various source mechanisms. Our objective is to find a source mechanism best matching the EST waveforms. This source mechanism may be found using a forward modeling approach or an inversion approach by solving (8). The question that we will address in the following is whether the EST algorithm enables us to use the shorter period surface wave energy to reliably determine the source mechanism solution.

We found that for most of the stations the data from event II have higher signal-to-noise ratio than for event III. This may be related to weather conditions in the summer for many stations for event III or may reflect the difference in magnitude. The event II data set is also much larger, since it includes many recently deployed stations. In the following analysis we use the EST waveforms derived with event II as the auxiliary event, although the EST waveforms obtained with event III as the auxiliary event yield essentially the same results, indicating the reliability of source parameters of these auxiliary events. In the calculation of the EST waveforms, the synthetics for event II are computed for a point source with a step-time function located at the hypocenter and the corresponding RWI1 mechanism. Given several auxiliary events, one could stack the EST waveforms to reduce sensitivity to auxiliary event mechanisms, but we have not attempted that here.

We compare the EST waveforms with synthetics computed for the primary event for a point source located at the epicenter with a half duration of 5 s at a depth of 14 km. A 14-km centroid depth was obtained from the regional waveform inversions for the Northridge mainshock [*Dreger*, 1994].

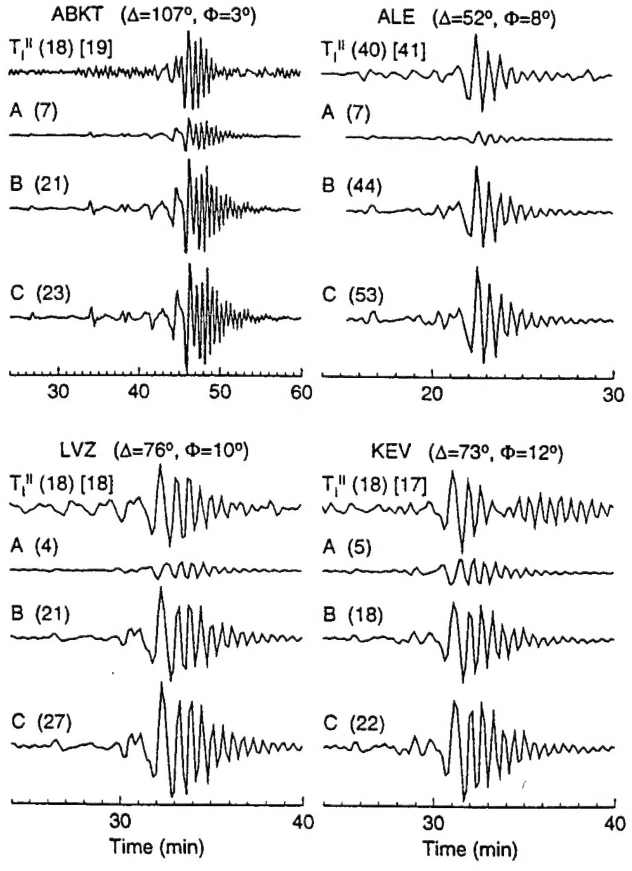


**Figure 4.** Transverse components of EST waveforms ($T_I^{II}$) for the Northridge mainshock at various stations, which are obtained with the synthetics for the auxiliary event (II) being computed for the focal mechanism from regional wave inversions. Amplitudes are given in parentheses in units of microns (amplitudes of $T_I^{II}$ with the synthetics computed for the focal mechanism from $P$ wave first motions are shown in brackets for comparison). Symbols A, B, and C indicate synthetics computed for the Northridge mainshock for a seismic moment of $1.2 \times 10^{19}$ N m and various focal mechanisms listed in Table 1: first motion solution, A; regional wave solution, B; and CMT solution, C.

Now we determine which mechanism listed in Table 1 best matches the EST signals for the mainshock. In comparison with the RWI1 model the RWI2 model differs more from the fault geometry that is inferred from the aftershock distribution (Figure 2); for simplicity the RWI2 model is not discussed here. Figure 4 shows the transverse components of the EST waveforms, along with synthetics for several stations in the azimuth range 3° to 12°. These signals are dominated by Love waves. For each station the synthetics for different source mechanisms have similar waveforms, indicating that variations of the instantaneous phase for surface waves are not sensitive to the modest difference between these source mechanisms. However, the synthetic amplitudes vary substantially. The amplitudes of the synthetics for the RWI1 mechanism (mechanism B in Figure 4) have the best agreement with the EST amplitudes. For other stations, differences between amplitudes of the synthetics for these different source mechanisms are smaller than for the stations shown in Figure 4.

In order to examine the sensitivity of the amplitudes of the synthetics to the dip, strike, and rake of the south dipping nodal plane, we computed synthetic seismograms for many more source mechanisms. We found that for the transverse component seismograms at the stations shown in Figure 4, the amplitudes of the synthetics are mainly sensitive to the strike of the nodal plane, reflecting the fact that these stations are located near the nodal direction of the Love wave radiation pattern for the Northridge earthquake. This indicates that the amplitudes of Love waves are useful for resolving the strike direction for thrust fault earthquakes when the EST algorithm is used. For the transverse components of EST waveforms our forward modeling analysis indicates that the strike of the south dipping nodal plane is between 110° and 120°, compatible with the aftershock distributions (Figure 2).

The EST waveforms shown in Figure 4 are computed using the RWI1 mechanism for the auxiliary event. We also computed EST waveforms using the PFM mechanism for the auxiliary event, which differs in the strike of the south dipping nodal plane by 16° from the RWI1 mechanism. We found that the amplitudes of the EST waveforms are not very dependent on this choice, demonstrating the stability of EST waveforms relative to small differences in the source mechanism for the auxiliary event. This indicates that using EST waveforms to constrain the source mechanism of the primary event is a robust approach, as long as uncertainties in the auxiliary event mechanism are not too large.

Because of the nonlinear relation between data and fault parameters strike, dip, and rake, it is very complicated to quantify error estimates for the primary event fault parameters associated with small perturbations in the auxiliary event fault parameters; but this is offset by the advantage of being able to quantify error estimates for moment tensor elements, as discussed in the previous section, and by being able to very closely model the EST waveforms.

We also model vertical components of the EST waveforms. The vertical and radial components are dominated by Rayleigh waves. For the data set used in this study, the radial components have poor signal-to-noise ratios and are not used for the forward modeling. Figure 5 shows the vertical components of the EST waveforms along with synthetics computed for different source mechanisms for stations at various azimuths.

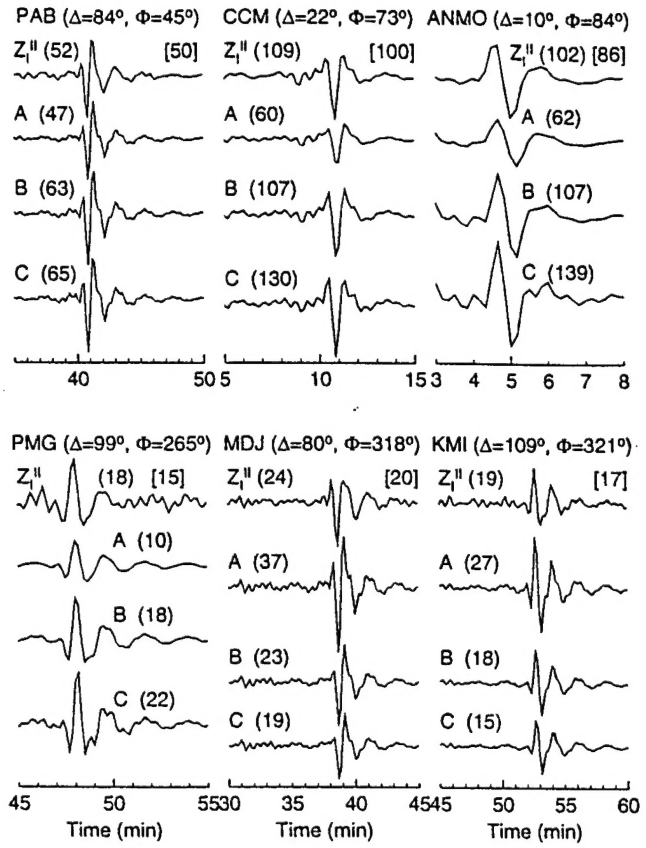


**Figure 5.** Similar to Figure 5 for vertical components of EST waveforms for various stations.

The data shown here represent a small portion of the entire data set; however, these are the most sensitive to the source mechanisms discussed here and have higher signal-to-noise ratios than data at other stations. Analysis of these Rayleigh wave waveforms yields the same conclusion as our analysis of the transverse components: for most of the stations the amplitudes of the synthetics for the RWI1 mechanism best fit the EST amplitudes in comparison with the PFM and CMT mechanisms. For station PAB (San Pablo, Spain), however, the PFM mechanism is preferred over the RWI1 mechanism (Figure 5). Note that for this station the variation of the amplitude of the synthetics for different source mechanisms is relatively small in comparison with that for other stations.

The EST waveforms shown in Figures 4 and 5 correspond to some of the highest signal-to-noise ratio data for both primary and auxiliary events. We believe that the forward modeling approach used above is robust, although qualitative, in discriminating between candidate source mechanisms of the Northridge mainshock. It is difficult to estimate the uncertainty of the amplitude of the EST waveforms quantitatively. Errors may arise from the separation of the hypocentral location of the primary and auxiliary events, inaccuracy of the source mechanism of the auxiliary event, or from station noise. It is clear that the EST algorithm works better for stations at close distances to the source. For stations ALE (Δ=52°), CCM (22°), and ANMO (10°), the fit of the synthetics to the EST waveforms is much better than for stations at larger distances. This may be explained by the fact that assumption (7) is more robust for regional seismic waves than for teleseismic waves, or simply by the better signal-to-noise ratio.

For comparison with the forward modeling analysis described above, we inverted the EST waveforms for the moment tensor using the CMT inversion method [*Dziewonski et al.*, 1981]. Our data set included vertical, transverse, and radial components for a total of 31 stations and 64 channels. Many stations clustered along the azimuth range between 210° and 240° (mostly in China) were eliminated to obtain uniform azimuthal coverage. Our moment tensor solution (hereinafter referred to as EST solution) is essentially a double couple with strike, $\phi$ = 115°, dip, $\delta$ = 40°, and rake, $\lambda$ = 95° for the south dipping nodal plane (the fault plane) and $\phi$ = 289°, $\delta$ = 50°, and $\lambda$ = 86° for the north dipping nodal plane (Figure 2 and Table 2). The EST solution has a nondouble couple component less than 1%, which is smaller than for the routine CMT solution (about 5%).

This mechanism is in close agreement with the combined source model obtained by *Wald et al.* [1996] from joint inversion of strong-motion, teleseismic, and GPS data, and the source model determined independently by *Hudnut et al.* [1996] from GPS data, and aftershock distribution. It differs somewhat from solutions for *P* wave first motions and routine CMT inversion (Figure 2 and Table 2). Using the aftershock distribution, we estimated the fault dip at between 37° and 42° and fault strike at between 105° and 120° (Figure 2). In the combined source model of *Wald et al.* [1996], the rake is independently determined, while the strike and dip are inferred from the aftershock distribution. By comparing the EST solution with the combined source model, the fault model from the geodetic data analysis, and aftershock distributions, we estimate the uncertainties for the strike, dip, and rake in our EST solution at less than 5° (Figure 2).

The centroid depth from the inversion is about 12 km, which is 2 km deeper than for the auxiliary event (event II). This depth is in excellent agreement with the combined source model obtained by *Wald et al.* [1996] but is slightly deeper than the 10 km centroid depth obtained by *Hudnut et al.* [1996] from GPS data and shallower than the 14 km centroid depth obtained by *Dreger* [1994] from regional waveform inversions (Figure 2). We estimate the uncertainty of the depth in the EST solution at less than 2 km, although this is weakly dependent on our choice of PREM as a reference model. As discussed previously, the uncertainty of the estimate of the primary event centroid depth reflects uncertainties of the auxiliary event centroid estimates and is independent of errors in the prescribed source mechanism of the auxiliary event.

The centroid location obtained from the CMT inversion of EST waveforms is about 5 km to the north of the epicenter, which is also in close agreement with the direction of main rupture directivity [*Wald et al.*, 1996; *Zeng and Anderson*, 1996]. The epicentral (or centroidal) estimate obtained here is subject to errors in the prescribed source depth and mechanism of the auxiliary event; however, it is consistent with the analysis of combined strong-motion, teleseismic, and GPS data. While the EST results for the Northridge event are not surprising, they do represent a validation of the EST methodology and a refinement of the teleseismic point-source solution which brings it to better agreement with independent constraints. The methodology exploits the mechanism and depth sensitivity of 30-140 s surface waves, which are usually ignored. The methodology offers most promise in application to remote areas where large events can be used as auxiliary events to process solutions for small events recorded at only a few stations.

## Discussion

The significance of using the EST procedure in earthquake source studies is the reduction of propagation effects of Earth's lateral and radial heterogeneities that are not predicted by a reference Earth model. The path calibration is made for complete waveforms and for each path to optimize the performance of source inversion methods. The calibration allows us to make use of 30-140 s waves, which may be so strongly affected by the complexity of the Earth's structure that direct inversion of the signals is not possible.

The EST algorithm can be applied to analysis of source parameters of a large earthquake using a small earthquake with well-constrained source mechanism as the auxiliary event, as demonstrated in this study. However, for optimal performance of the algorithm it is preferable to use an auxiliary event which is larger than the primary event. Since errors in auxiliary event data will project into EST waveforms, using a large auxiliary event allows us to enhance the signal-to-noise ratio in the EST waveforms. Moreover, source mechanisms of large events are usually more reliable, because they can be better constrained by larger number of recordings. In this study we used two earthquakes with different centroid and source mechanism estimates as the auxiliary event, the purpose being to test the reliability of the EST algorithm. However, the algorithm requires only one auxiliary event.

The EST procedure holds promise for reliable source inversion for small earthquakes in a calibrated region. Since small events of $m_b$ of 4 or less are recorded only at local or regional distances and only have good signal-to-noise ratio in passbands with periods less than about 40 s, path calibration is essential. In practice, it is necessary to use an accurate model of the crustal structure in the calculation of synthetics for the auxiliary event in order to exploit the short-period energy. The crustal structure can be estimated using data from large, auxiliary events in the region. The source mechanisms of these events must be independently determined, perhaps by teleseismic signals, to avoid circularity in modeling the regional waveforms. This is possible because large events produce adequate teleseismic signals. Depths of the events can be constrained robustly using teleseismic body waves and regional sP-P times [*Langston*, 1994]. If one has a suite of large events with well-constrained source parameters, the EST method can be used to develop spatially varying deconvolution filters to allow small events to be inverted throughout the region.

This study was partly motivated by the fact that source inversions of teleseismic surface waves with aspherical model corrections do not always yield a solution compatible with independently determined solutions, and partly by a desire to use an unexploited portion of the waveforms. In our previous CMT-type analysis of the source mechanism of the Northridge earthquake [*Zhang et al.*, 1994], we found that for body waves low-pass filtered with a 30-s cutoff period and surface waves low-pass filtered with a 135-s cutoff period, separate inversions gave a body wave mechanism that is significantly rotated relative to the surface wave mechanism, while a simultaneous inversion yielded intermediate parameters, consistent with the independent solution obtained from regional waveform inversions [*Dreger*, 1994]. One interpretation for the discrepancy between body and surface wave inversions involves changes in the source mechanism during rupture, sensed to a different degree by different wave types. Alternatively, the inconsistency may reflect different model errors in the inversions.

We also found discrepancies between inversions of only Rayleigh waves and joint inversions of Rayleigh and Love waves. While joint inversions yield solutions with a shallow-dipping north plunging nodal plane, Rayleigh wave inversions prefer solutions with a shallow-dipping south plunging nodal plane. This discrepancy is most likely due to inaccuracy of the Earth model involved in the source determination. Love waves usually have smaller signal-to-noise ratio than Rayleigh waves, thus including Love waves in inversions may increase uncertainty relative to inversions that use only Rayleigh waves. Love waves also commonly show larger deviations from predictions for standard Earth models than do Rayleigh waves. The greater variance in Love wave observations may cause different biases in resolving the true source radiation pattern, resulting in an apparent Rayleigh-Love discrepancy. Therefore including Love waves in inversions does not necessarily provide improved source mechanism resolution, unless propagation errors are reduced to a comparable level. Aspherical Earth model corrections did reduce the discrepancies between inversions of different surface wave data sets, but not to a significant extent. The limited accuracy of the aspherical corrections at long period (150 s and longer) and the low signal-to-noise ratio for the long-period Love waves still preclude a consistent inversion. Similar problems were analyzed by *Kuge et al.* [1996] for the July 12, 1993, Hokkaido-Nansei-Oki, Japan, earthquake.

The objective of the procedure introduced in this study is to reduce the biases due to the effects of Earth's lateral and radial heterogeneity in the source determination and to extend the passband beyond that possible with existing low-resolution aspherical models. The key to success is independent knowledge of the auxiliary event's source mechanism and depth. The advantage of the method is that it enables use of much more complete waveform information than possible with theoretical propagation models.

In comparison with the discrepancy discussed above between results obtained from observed Rayleigh and Love waves, more consistent results are obtained from EST waveforms for only Rayleigh waves and from EST waveforms for both Rayleigh and Love waves. The EST approach appears to work better for stations at short distances, presumably due to both the higher signal-to-noise ratio and reduced levels of highly path dependent multipathing. The method allows broadband surface wave information to contribute to the source inversion and can complement empirical Green's function methods used for estimating the source time function [e.g., *Murphy*, 1977; *Hartzell*, 1978; *Frankel et al.*, 1986; *Ammon et al.*, 1993; *Li and Toksöz*, 1993].

The limitations of the EST algorithm involve the fact that the source mechanism of the auxiliary event must be known a priori and that event must be large enough so that 30-140 s surface waves are well recorded at stations that also record the primary event. For remote areas, using large earthquakes reported in the Harvard CMT catalog is often the only choice for the auxiliary event. In addition, the spectral division in the calculation of the EST waveform often limits the resolution of the method. The choice of method used for reducing error in the deconvolution is subject to how well the detailed characteristics of the signal and noise are known. In order to overcome these limitations, the EST algorithm may be extended to include multiple auxiliary events to optimize the deconvolution filter for the primary event; and it is also desirable to develop highly accurate deconvolution techniques.

Although routine CMT analysis or $P$ wave first motion analysis can provide acceptable source parameter determinations for study of global and regional seismicity, we feel that it is warranted to identify the error bounds associated with various determinations and to resolve differences between these routine determinations. This is particularly valuable when there are other types of seismological and geophysical data available for important events such as the Northridge earthquake. Using this event as a calibration of the EST procedure, we find a solution consistent with strong motions, teleseismic and regional waveforms, geodetic measurements, and aftershock distributions. This gives us confidence for application of the methodology to other events and contributes to the overall characterization of the Northridge earthquake.

## Conclusions

The Earth simplifying transformation (EST) technique allows complete teleseismic waveform information in the period range 30 to 140 s to be used to constrain earthquake source parameters. Normally, the propagation effects of Earth's lateral and radial heterogeneities are so severe that teleseismic intermediate- and short-period surface waves are not used to study the earthquake source despite their superb signal-to-noise ratio and sensitivity to source depth. The method involves empirical path calibration and requires independent constraints on the source parameters of at least one auxiliary event. The method can be applied to events either larger or smaller than the calibration event, and regional or teleseismic phases can be used. Using two well-constrained, moderate-size earthquakes in southern California, we apply the EST method to successfully resolve the source parameters for the January 17, 1994, Northridge, California, earthquake. Our solution, obtained using wave field information that is usually filtered out of standard inversions, is in close agreement with the results of a joint inversion of strong-motion, teleseismic, and GPS data. It differs somewhat from solutions for $P$ wave first motions and routine CMT inversion and appears to eliminate biases affecting these solutions. The EST procedure enables much more complete teleseismic waveform information to be used in constraining the source mechanism of moderate size earthquakes ($m_b$ 4 or larger), as long as recordings for a nearby event with a well-determined mechanism are available. The auxiliary event may be either larger or smaller than the primary event, and multiple auxiliary events can be used to spatially interpolate the deconvolution filters. The EST method holds promise for enabling complete waveform inversion for small- and moderate-size events in a region calibrated by a few well-studied auxiliary events.

**Acknowledgments.** The data used in this study were made available by courtesy of the IRIS/DMC. We thank G. H. Sutton, D. Doser, A. L. Bent, and the anonymous reviewer for helpful comments. This work was supported by NSF grants EAR-9219922 and EAR-9416342 and by AFOSR grant F49620-94-1-0315. Contribution 287 of the W. M. Keck Seismological Laboratory and the Institute of Tectonics, University of California, Santa Cruz.

## References

Ammon, C. J., A. A. Velasco, and T. Lay, Rapid determination of rupture directivity: Application to the 1992 Landers ($M_s$ = 7.4) and Cape Mendocino ($M_s$ = 7.2), California, earthquakes, *Geophys. Res. Lett., 20*, 97-100, 1993.

Bent, A. L., and D. V. Helmberger, Source complexity of the October 1, 1987, Whittier Narrows earthquake, *J. Geophys. Res., 94*, 9548-9556, 1989.

Bent, A. L., D. V. Helmberger, R. J. Stead, and P. Ho-Liu, Waveform modeling of the November 1987 Superstition Hills earthquakes, *Bull. Seismol. Soc. Am., 79*, 500-514, 1989.

Dreger, D. S., Empirical Greens function study of the January 17, 1994, Northridge, California, earthquake, *Geophys. Res. Lett., 21*, 2633-2636, 1994.

Dreger, D. S., and D. V. Helmberger, Source parameters of the Sierra Madre earthquake from regional and local body waves, *Geophys. Res. Lett., 18*, 2015-2018, 1991.

Dziewonski, A. M., and D. L. Anderson, Preliminary reference Earth model, *Phys. Earth Planet. Inter., 25*, 297-356, 1981.

Dziewonski, A. M., T.-A. Chou, and J. H. Woodhouse, Determination of earthquake source parameters from waveform data for studies of global and regional seismicity, *J. Geophys. Res., 86*, 2825-2852, 1981.

Dziewonski, A. M., G. Ekström, and M. P. Salganik, Centroid-moment tensor solutions for April-June 1991, *Phys. Earth Planet. Inter., 71*, 6-14, 1992.

Dziewonski, A. M., G. Ekström, and M. P. Salganik, Centroid-moment tensor solutions for January-March 1994, *Phys. Earth Planet. Inter., 86*, 253-261, 1994.

Frankel, A., J. Fletcher, F. Vernon, L. Haar, J. Berge, T. Hanks, and J. Brune, Rupture characteristics and tomographic source imaging of $M_L$ ~ 3 earthquake near Anza, south California, *J. Geophys. Res., 91*, 12,633-12,650, 1986.

Gilbert, F., and A. M. Dziewonski, An application of normal mode theory to the retrieval of structure parameters and source mechanisms from seismic spectra, *Philos. Trans. R. Soc. London, Ser. A, 278*, 187-269, 1975.

Hartzell, S. H., Earthquake aftershocks as Green's functions, *Geophys. Res. Lett., 5*, 1-4, 1978.

Hauksson, E., The 1991 Sierra Madre earthquake sequence in southern California: Seismological and tectonic analysis, *Bull. Seismol. Soc. Am., 84*, 1058-1074, 1994.

Hauksson, E., L. Jones, and K. Hutton, The 1994 Northridge earthquake sequence in California: Seismological and tectonic aspects, *J. Geophys. Res., 100*, 12,335-12,355, 1995.

Hudnut, K. W., *et al.*, Co-seismic displacements of the 1994 Northridge, California, earthquake, *Bull. Seismol. Soc. Am., 86*, S19-S36, 1996.

Kanamori, H., J. Mori, and T. Heaton, The 3 December 1988, Pasadena earthquake ($M_L$ = 4.9) recorded with the very broadband system in Pasadena, *Bull. Seismol. Soc. Am., 80*, 483-487, 1990.

Kanamori, H., H.-K. Thio, D. S. Dreger, and E. Hauksson, Initial investigation of the Landers, California, earthquake of 28 June 1992 using TERRAscope, *Geophys. Res. Lett., 19*, 2267-2270, 1992.

Kuge, K., J. Zhang, and M. Kikuchi, The 12 July 1993 Hokkaido-Nansei-Oki, Japan, earthquake: Effects of source complexity on surface-wave radiation, *Bull. Seismol. Soc. Am., 86*, 505-518, 1996.

Langston, C. A., An integrated study of crustal structure and regional wave propagation for southeastern Missouri, *Bull. Seismol. Soc. Am., 84*, 105-118, 1994.

Li, Y., and N. M. Toksöz, Study of the source process of the 1992 Colombia $M_s$ = 7.3 earthquake with the empirical Green's function method, *Geophys. Res. Lett., 20*, 1087-1090, 1993.

Murphy, J. R., Seismic source functions and magnitude determinations for underground nuclear detonations, *Bull. Seismol. Soc. Am., 67*, 135-158, 1977.

Pasyanos, M. E., D. S. Dreger, and B. Romanowicz, Toward real-time estimation of regional moment tensors, *Bull. Seismol. Soc. Am., 86*, 1255-1269, 1996.

Patton, H., Reference point equalization method for determining the source and path effects of surface waves, *J. Geophys. Res., 85*, 821-848, 1980.

Patton, H. J., and G. Zandt, Seismic moment tensors of western U.S. earthquakes and implications for the tectonic stress field, *J. Geophys. Res., 96*, 18,245-18,259, 1991.

Ritsema, J., and T. Lay, Long-period regional wave moment tensor inversion for earthquakes in the western United States, *J. Geophys. Res., 100*, 9853-9864, 1995.

Romanowicz, B., G. Anderson, L. Gee, R. McKenzie, D. Neuhauser, M. Pasyanos, and R. Uhrhammer, Real-time seismology at U.C. Berkeley (abstract), *Eos Trans. AGU, 73* (43), Fall Meet. Suppl., 69, 1992.

Romanowicz, B., D. S. Dreger, M. Pasyanos, and R. Uhrhammer, Monitoring of strain release in central and northern California using broadband data, *Geophys. Res. Lett., 20*, 1643-1646, 1993.

Romanowicz, B., D. Neuhauser, B. Bogaert, and D. Oppenheimer, Accessing northern California earthquake data via internet, *Eos Trans. AGU, 75* (23), 257, 259-260, 1994.

Shen, Z.-K., B. X. Ge, D. D. Jackson, D. Potter, M. Cline, and L.-Y. Sung, Northridge earthquake rupture models based on the Global Positioning System measurements, *Bull. Seismol. Soc. Am., 86*, S37-S48, 1996.

Song, X. J., L. E. Jones, and D. V. Helmberger, Source characteristics of the 17 January 1994 Northridge, California, earthquake from regional broadband modeling, *Bull. Seismol. Soc. Am., 85*, 1591-1603, 1995.

Thio, H.-K., and H. Kanamori, Moment tensor inversions for local earthquakes using surface waves recorded at TERRAscope, *Bull. Seismol. Soc. Am., 85*, 1021-1038, 1995.

Thio, H.-K., and H. Kanamori, Source complexity of the 1994 Northridge earthquake and its relation to aftershock mechanisms, *Bull. Seismol. Soc. Am., 86*, S84-S92, 1996.

Uhrhammer, R. A., Broadband near-field moment tensor inversions (abstract), *Eos Trans. AGU, 73* (43), Fall Meet. Suppl., 375, 1992.

Uhrhammer, R. A., D. S. Dreger, M. Pasyanos, and B. Romanowicz, Rapid moment tensor estimation using regional data (abstract), *Eos Trans. AGU, 75* (44), Fall Meet. Suppl., 481, 1994.

Wald, D. J., and T. H. Heaton, A dislocation model of the 1994 Northridge, California, earthquake determined from strong ground motions, *U.S. Geol. Surv. Open File Rep., 94-278*, 1994.

Wald, D. J., D. V. Helmberger, and S. H. Hartzell, Rupture process of the 1987 Superstition Hills earthquake from the inversion of strong-motion data, *Bull. Seismol. Soc. Am., 80*, 1079-1098, 1990.

Wald, D. J., T. H. Heaton, and K. W. Hudnut, The slip history of the 1994 Northridge, California, earthquake determined from strong-motion, teleseismic, GPS, and leveling data, *Bull. Seismol. Soc. Am., 86*, S49-S70, 1996.

Weidner, D. J., and K. Aki, Focal depth and mechanism of mid-ocean ridge earthquakes, *J. Geophys. Res., 78*, 1818-1831, 1973.

Zeng, Y., and J. G. Anderson, A composite source model for the 1994 Northridge earthquake using genetic algorithms, *Bull. Seismol. Soc. Am., 86*, S71-S83, 1996.

Zhang, J., S. Tsuboi, and T. Lay, Analysis of broadband far-field seismic data for the January 17, 1994, Northridge, California, earthquake (abstract), *Eos Trans. AGU, 75* (44), Fall Meet. Suppl., 171, 1994.

Zhao, L.-S., and D. V. Helmberger, Source estimation from broadband regional seismograms, *Bull. Seismol. Soc. Am., 84*, 91-104, 1994.

K. Kuge, Department of Geophysics, Kyoto University, Kyoto, 606-01 Japan.

T. Lay and J. Zhang, Institute of Tectonics and W. M. Keck Seismological Laboratory, University of California, Santa Cruz, CA 95064. (e-mail: zan@earthsci.ucsc.edu)

S. Tsuboi, Department of Geoscience, National Defense Academy, Yokosuka, 239 Japan.

(Received August 12, 1996; revised December 4, 1996;
accepted December 11, 1996.)

Bulletin of the Seismological Society of America, Vol. 87, No. 4, pp. 832–846, August 1997

# Source Characterization Using Simplified Waveforms: Tests on Earthquakes and Nuclear Explosions in Xinjiang, China

by Jiajun Zhang

**Abstract** Complete waveforms with periods longer than 30 sec recorded at teleseismic and regional distances are used to characterize the source of several earthquakes and underground nuclear explosions in the Lop Nor area, Xinjiang, China. Propagation effects of Earth's heterogeneities on data for several auxiliary events with well-constrained source mechanisms, in the vicinity of the primary event, are calibrated by frequency-domain division of each pair of observed and synthetic waveforms, with the synthetics being computed for a reference Earth model. The frequency-dependent deconvolution filters obtained for the auxiliary events are interpolated to construct a predicted deconvolution filter, which is convolved with observed waveforms for the primary event to remove the empirically determined propagation effects and to obtain simplified waveforms that are intrinsically well predicted by the reference Earth model. These waveforms are then inverted for the source mechanism and centroid time, location, and depth of the primary event. The inversion yields a centroid depth of 13 km for the 7 September 1994 earthquake ($m_b$ = 5.1), significantly shallower than the 33-km depth reported previously from routine determinations. The centroid depth of the 5 October 1993 nuclear explosion plus tectonic release is estimated at approximately 4 km, while the depth of the 21 May 1992 explosion plus tectonic release is less well resolved and may be deeper than 5 km, reflecting limited resolution of the passband used here. With extension to shorter-period energy, the method holds promise for reliable source inversion for small events in a calibrated region.

## Introduction

Many recent underground nuclear explosions at the Lop Nor test site in Xinjiang, China, were well recorded by broadband instruments from global and regional seismic networks and reported in various seismological catalogs, such as the Preliminary Determination of Epicenters Catalog (PDE) from NEIC. The underground nuclear explosions that occurred during the period of 1969 to 1992 were registered with $m_b$ magnitudes between 4.4 and 6.5 (Matzko, 1992). As reported in PDE, several recent earthquakes with $m_b$ about 4 occurred in the test-site area. The determination of hypocentral locations and focal mechanisms of explosions and earthquakes in the area, as well as other less well-studied regions, where seismicity is low and previous geophysical studies are few, is of importance for monitoring nuclear explosions and for extending the fault-mechanism data base to these remote regions.

The Lop Nor test site is located in an intermontane basin and surrounding hills (Matzko, 1992, 1994), within an uplifted and mountainous terrain between the Turfan basin and the Tarim basin in Xinjiang (Fig. 1). The uplifted terrain is the southeastern extension of mountain massifs of Tien Shan. The Lop Nor lake, which has been dried up entirely since 1964, lies to the south in the northeastern part of the Tarim basin, and the Bosten Lake lies to the west of the terrain.

Moderate and large earthquakes frequently occur along margins of major basins and mountain ranges in Xinjiang, in particular, along the northern part of Tien Shan mountains to the west of Urumqi and the northern part of the Tarim basin to the west of the Bosten Lake. However, for the eastern part of the Tarim basin and the region between Turfan and Tarim basins, the seismic activity has been low since 1600, with earthquake magnitudes being, in general, smaller than 6 (Hu *et al.*, 1989).

To provide a means of identifying nuclear explosions from seismic recordings at regional and teleseismic distances, various techniques have been developed since the late 1950s (e.g., Brune and Pomeroy, 1963; Toksöz *et al.*, 1964; Murphy and Mueller, 1971; Helmberger and Harkrider, 1973; Lay *et al.*, 1984; Wallace *et al.*, 1985; Patton, 1991). Many investigations demonstrated that the identification of underground explosions is often hampered by our

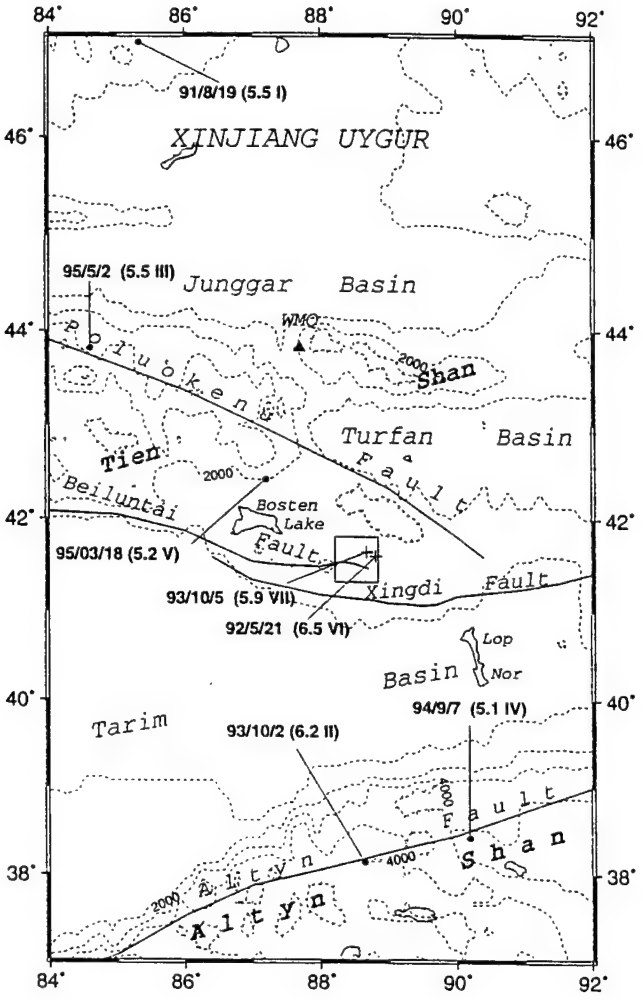


Figure 1. Map showing the Lop Nor, China, underground test site (box) and locations of nuclear explosions (crosses) and earthquakes (solid circles) used in this study. Body-wave magnitude $m_b$ and event numbers listed in Table 1 are shown in the parentheses for each event. Station location for WMQ is shown with the solid triangle. Active faults in the area are from Hu *et al.* (1989).

limited theoretical understanding of seismic wave propagation and generation by various types of sources (Aki and Tsai, 1972; Wallace, 1991; Patton, 1991; Murphy, 1995).

Accurately characterizing source properties of events that occurred in Central Asia requires detailed knowledge of wave-propagation effects, which may vary considerably between different paths. Given large variations in crustal thickness and upper mantle structure in the region revealed from analysis of various geophysical and geological data (Wu and Levshin, 1994), it is not surprising that seismic waves propagating in Central Asia show strong variations of amplitude and phase anomalies. The Tarim basin is the largest inland basin in China, lying in the innermost part of the vast territory that encompasses high mountain systems of Central Asia, which include Tien Shan, Pamir, and Hindu Kush to the north and west, and Karakoram, Kunlun, and Tibetan Plateau to the south of the basin.

In order to optimize the performance of source-inversion methods and to improve the resolution of source properties of seismic events in the Lop Nor area, in this study, we use a procedure to calibrate and remove waveform complexities due to effects of Earth's structure on wave propagation, with the calibration being made for each wave-propagation path and for complete waveforms. This procedure constitutes a complete waveform generalization of empirical path correction methods such as those of Weidner and Aki (1973) and Patton (1980a) and involves a noise-desensitized deconvolution technique, which differs from other commonly used methods. In the analysis of source parameters of a given seismic event (hereafter referred to as the primary event), the procedure consists of the following steps.

First, we compute synthetics for a reference Earth model using *a priori,* well-constrained focal mechanisms for several calibration or auxiliary events, which may be either larger or smaller than the primary event. The reference Earth model is chosen to be the best available model of Earth's structure for given data sets. By deconvolving the synthetic signals from data for every station auxiliary-event pair and component of seismograms, we obtain an observed, complex transfer function or deconvolution filter that represents the propagation effects that are not predicted by the reference Earth model for the specified station auxiliary-event and mechanism pair. Then we construct a predicted transfer function for the primary event for each station and component of seismograms by interpolating the observed transfer functions for the auxiliary events with a polynomial defined in the three-dimensional space of the hypocentral location and depth. Using the predicted transfer function, we remove the empirically determined propagation effects in a noise-desensitizing deconvolution procedure from the waveforms for the primary event, obtaining simplified waveforms that are well matched by the Earth model. These waveforms are then inverted for the centroidal parameters (centroid time, location, and depth) and moment tensor for the primary event using an iterative procedure.

To explore the resolution of source parameters using this method, we carried out several experiments on moment-tensor inversions for two recent nuclear explosions and two earthquakes that occurred in the vicinity of the Lop Nor test site, with the source parameters of one of the earthquakes being obtained previously but with unusually large uncertainties. In these experiments, we use data recorded at teleseismic and regional distances by Global Seismographic Network (GSN) stations, which do not include records of nuclear explosions for stations in China. With the exception of station WMQ, all the stations are located at epicentral distances larger than 8°. The data are dominated by high signal-to-noise ratio short-period surface waves, which we must accurately correct for propagation effects.

## Method

Following Gilbert and Dziewonski (1975), the spectrum of a component of ground motion excited by a point source at angular frequency $\omega$ for a reference Earth model may be given by

$$u'_k(\mathbf{x}, \mathbf{x}'_j, \omega) = \sum_{i=1}^{6} \psi_{ki}(\mathbf{x}, \mathbf{x}'_j, \omega) f'_i(\mathbf{x}'_j, \omega), \quad (1)$$

where $u'_k$ is the $k$th record in a set of seismograms, with the receiver at position $\mathbf{x}$ and the source at $\mathbf{x}'_j$; $\psi_{ki}$ are excitation coefficients; and $f'_i$ represent six independent components of the moment-rate tensor. In the following discussion, $\omega$ is ignored for expression simplicity. The question that we shall address in this study is as follows. Given a set of seismograms at common stations from an event at $\mathbf{x}_p$ (the primary event) and from $N$ events with known source parameters at $\mathbf{x}'_1, \ldots, \mathbf{x}'_N$ (auxiliary events), which are located in the proximity of $\mathbf{x}_p$, along with synthetics for the auxiliary events, $u'_k$, computed for a reference Earth model, is it possible to determine hypocenter position ($\mathbf{x}_p$) and moment-rate tensor ($f_i$) of the primary event?

Taking into account our imperfect knowledge of the Earth's structure and background noise, the spectra of observed ground motion for the auxiliary events may be expressed as

$$U'_k(\mathbf{x}, \mathbf{x}'_j) = u'_k(\mathbf{x}, \mathbf{x}'_j)\, \alpha'_k(\mathbf{x}, \mathbf{x}'_j) + \varepsilon'(\mathbf{x}, \mathbf{x}'_j) \qquad (j = 1, \ldots, N), \quad (2)$$

where $\alpha'$ represents the transfer function between the actual Earth's structure and the reference Earth model for a given station auxiliary-event pair, assuming that the source parameters of the auxiliary event are precisely known. In this analysis, we ignore the noise terms ($\varepsilon$) and search for functions $\alpha'_k$ (hereafter referred to as the observed transfer function) by solving the following equations:

$$\alpha'_k(\mathbf{x}, \mathbf{x}'_j) = U'_k(\mathbf{x}, \mathbf{x}'_j)/u'_k(\mathbf{x}, \mathbf{x}'_j) \qquad (j = 1, \ldots, N). \quad (3)$$

Since $\alpha'$ are not uniquely constrained by equations (3) and the auxiliary events span a region with very small volume near the Earth's surface, we will determine $\alpha'(\mathbf{x}, \mathbf{x}')$ for each station $\mathbf{x}$ using a polynomial of degree $N$-1 modified from the Lagrange interpolation formula (Dahlquist and Björck, 1974), which is defined in the three-dimensional space and bounded for any $\mathbf{x}'$. The coefficients of the polynomials are determined using (3) from data and synthetics for the auxiliary events. Then we may compute $\alpha'(\mathbf{x}, \mathbf{x}')$ for any $\mathbf{x}'$, say, the assumed position of the primary event, $\mathbf{x}_p$. This results in $\alpha'(\mathbf{x}, \mathbf{x}_p)$ (hereafter referred to as the predicted transfer function).

Using the value of $\alpha'(\mathbf{x}, \mathbf{x}_p)$ and the observed spectra for the primary event, $U_k(\mathbf{x}, \mathbf{x}_p)$, we define the following transformation:

$$u^p_k(\mathbf{x}, \mathbf{x}_p) = U_k(\mathbf{x}, \mathbf{x}_p)/\alpha'_k(\mathbf{x}, \mathbf{x}_p), \quad (4)$$

which is referred to as the Earth simplifying transformation (EST). Following the notation used in (1) and (2), the observed spectra for the primary event can be written as

$$U_k(\mathbf{x}, \mathbf{x}_p) = u_k(\mathbf{x}, \mathbf{x}_p)\, \alpha_k(\mathbf{x}, \mathbf{x}_p), \quad (5)$$

where the theoretical spectra are given by

$$u_k(\mathbf{x}, \mathbf{x}_p) = \sum_{i=1}^{6} \psi_{ki}(\mathbf{x}, \mathbf{x}_p) f_i(\mathbf{x}_p). \quad (6)$$

For a given data set, one must make a reasonable choice of the theory, so that corresponding $\alpha$ are slowly varying functions of the source position and the moment-rate tensor. This can be examined by comparing the differences between data and synthetics for various auxiliary events; if the differences are similar among auxiliary events, then the corresponding $\alpha$ are smooth functions. For a reasonable choice of the theory, we assume

$$\alpha_k(\mathbf{x}, \mathbf{x}_p) = \alpha'_k(\mathbf{x}, \mathbf{x}_p). \quad (7)$$

The accuracy of this assumption is influenced by the proximity of the events, the frequency content of the data, and our choice of the method used for calculation of the synthetics. Then it follows from (4) to (7) that

$$u^p_k(\mathbf{x}) = \sum_{i=1}^{6} \psi_{ki}(\mathbf{x}, \mathbf{x}_p) f_i(\mathbf{x}_p), \quad (8)$$

which is correct to first order in terms of $\alpha$'s Taylor series expansion and will be used to determine the hypocentral position ($\mathbf{x}_p$) and moment-rate tensor ($f_i$) of the primary event. For simplicity of analysis, we adopt a frequently used assumption: $f_i$ are considered to be independent of frequency, except for a common correction for an assumed duration of the source, and are regarded as the moment tensor. We will use an iterative procedure to determine the hypocentral depth, location, centroid time, and source moment tensor; in each iteration, first we solve equations (8) for the moment tensor, and then we calculate partial derivatives of seismograms and determine the perturbation of the depth, location, and centroid time using residual seismograms.

Errors in auxiliary-event moment tensors will project into the primary-event solution, so it is critical that the moment tensors of auxiliary events used here are well determined. In addition, one must select auxiliary events with data of good signal-to-noise ratio (SNR), since noise in the auxiliary-event data will affect EST waveforms for the primary event through the deconvolution filters.

In order to construct highly accurate deconvolution fil-

ters in the application of the EST algorithm, it is often preferred to use large auxiliary events rather than small ones. In general, data from large events usually show good SNR, and the source mechanisms of large events can be well constrained using more recordings so as to improve azimuthal, wave-type, and ray-parameter coverage. For these reasons, the uncertainties of estimates of source parameters of large events are usually smaller than those for small events, as indicated in routinely published catalogs. In the computation of synthetics for large events, one must take into account effects of source complexity due to finiteness. The effects are usually calculated using a source time function with a finite duration, while for some large events, the effects can be calculated using a unilateral or bilateral rupture model.

Note that for the EST algorithm involving only one auxiliary event, the EST waveform ($u_k^P$) depends linearly on the moment tensor ($f_i'$) of the auxiliary event. In the ideal case with data free of noise and multipathing effects, this will remove the sensitivity to the focal mechanism of the auxiliary event of the primary-event centroid estimates obtained from inversion of EST waveforms. Clearly, errors in auxiliary-event centroid estimates (time, location, and depth) will project into the primary-event solution, influencing not only centroid but also source-mechanism estimates, so good independent constraints on the auxiliary-event centroid parameters are critical. However, it is important to examine how errors in the auxiliary-event source mechanism project into the primary-event solution.

To address this question, we assume that the errors in the auxiliary-event source mechanism are $g_i' - f_i'$, where $f_i'$ is the correct moment tensor of the auxiliary event, and $g_i'$ is an incorrect, arbitrarily given moment tensor in the calculation of synthetics for the auxiliary event. The errors also can be described by bias factors $d_i$ with $g_i' = f_i' d_i (i = 1, \ldots, 6)$. Then the EST waveforms corresponding to the incorrect auxiliary-event moment tensor $g_i'$ may be written as

$$u_k^P(\mathbf{x}) = \sum_{i=1}^{6} \psi_{ki}(\mathbf{x}, \mathbf{x}_p)\, g_i\, (\mathbf{x}_p), \tag{9}$$

with $g_i = f_i d_i (i = 1, \ldots, 6)$, where $f_i$ is the correct moment tensor of the primary event. Clearly, one will recover a biased moment tensor ($g_i$) for the primary event, with the bias factors ($d_i$) being the same as those for the auxiliary-event moment tensor.

However, since both the EST waveforms in (9) and (8) correspond to the same set of excitation coefficients, inversions of biased EST waveforms (9) will yield the same centroid estimates as for correct EST waveforms (8), reflecting the stability of centroidal solutions obtained from EST waveforms. Therefore, errors in the auxiliary-event source mechanism do not project into errors in the primary-event centroid estimates. It follows that using well-determined centroid parameters of the auxiliary event, reliable centroid parameters of the primary event can be obtained by inverting EST waveforms, even if the EST waveforms are computed for an incorrect, arbitrarily given auxiliary-event moment tensor. Our experiments on the 7 September 1994 earthquake data set confirm that variation of the prescribed auxiliary-event moment tensor does not affect the primary-event centroid estimate. In the following section, we will utilize the stability of centroidal solution from inversion of EST waveforms discussed here in the experiments to determine the apparent depth of explosion plus tectonic release of the 5 October 1993 explosion relative to that of the 21 May 1992 explosion.

While in conventional methods the errors of the moment-tensor solution depend on model uncertainties, which are usually not well understood, in the EST algorithm, the errors of the primary-event moment-tensor solution depend mainly on the errors of the auxiliary-event moment tensor. When the biases in the auxiliary-event moment tensor are known, we can make use of the linear dependence of the derived primary-event moment tensor on the prescribed auxiliary-event moment tensor to estimate any possible biases in the primary-event moment-tensor solution. This is achieved by first estimating bias factors $d_i$ for the prescribed auxiliary-event moment tensor and then calculating the resulting errors in the primary-event moment-tensor solution: $g_i - g_i/d_i (i = 1, \ldots, 6)$.

## Tests

To test the algorithm described above, we carried out a series of experiments on the determination of source parameters of two nuclear explosions and two recent earthquakes that occurred in the vicinity of the Lop Nor underground test site (Table 1) using data sets of both teleseismic and regional waveforms. The first explosion occurred on 21 May 1992, with $m_b = 6.5$, the largest underground nuclear test in China. The second explosion occurred on 5 October 1993 and has $m_b = 5.9$. The two earthquakes occurred on 7 September 1994 and 18 March 1995, with $m_b$ of 5.1 and 5.2. The auxiliary events used in this study are listed in Table 1, their Harvard centroid-moment-tensor (CMT) solutions are listed in Table 2, and their focal mechanisms are shown in Figure 2.

For simplicity of the experiments, the synthetics are computed using the laterally homogeneous Earth model PREM (Dziewonski and Anderson, 1981) based on the normal-mode theory of Gilbert and Dziewonski (1975). Using this standard Earth model allows us to compare the performance of the EST algorithm with that for other methods commonly used in analysis of global seismicity.

Each record in our data set begins at the first arrival and includes minor-arc fundamental-mode surface waves, and is bandpass filtered between 30 and 50 sec before deconvolution. At longer periods, the SNR becomes small for most records used here, while the shortest period for the normal-mode data set used in this study is about 30 sec. Although the resolution of source properties using the EST algorithm is limited by our choice of the method in calculation of synthetics and the noise level inherent in our data set, we are

Table 1
Hypocentral Parameters of Events Used in This Study*

| Event | Date | Time | $m_b$ | Depth (km) | Lat (°N) | Long (°E) | Remarks† | |
|---|---|---|---|---|---|---|---|---|
| I | 91/08/19 | 06:05:51.3 | 5.5 | 30 | 46.944 | 85.302 | EQ | Aux |
| II | 93/10/02 | 08:42:32.7 | 6.2 | 14 | 38.190 | 88.663 | EQ | Aux |
| III | 95/05/02 | 11:48:11.6 | 5.5 | 33 | 43.776 | 84.660 | EQ | Aux |
| IV | 94/09/07 | 13:56:25.2 | 5.1 | 33 | 38.491 | 90.345 | EQ | Pr |
| V | 95/03/18 | 18:02:36.6 | 5.2 | 22 | 42.422 | 87.199 | EQ | Pr |
| VI | 92/05/21 | 04:59:57.5 | 6.5 | | 41.604 | 88.813 | Exp | Pr |
| VII | 93/10/05 | 01:59:56.5 | 5.9 | | 41.647 | 88.681 | Exp | Pr |

*From PDE monthly listings.
†EQ, earthquake; Exp, underground nuclear explosion at the Lop Nor test site; Aux, auxiliary or calibration event; Pr; primary or target event, which is analyzed in this study.

Table 2
Earthquake Source Parameters Used in This Study

| Event | Depth (km) | Best Double Couple | | | | | | | Remarks* |
|---|---|---|---|---|---|---|---|---|---|
| | | $M_w$ | Strike | Dip | Slip | Strike | Dip | Slip | |
| I | 55 | 5.24 | 68 | 36 | 51 | 293 | 63 | 114 | CMT |
| II | 15 | 6.08 | 82 | 68 | 53 | 326 | 42 | 146 | CMT |
| III | 18 | 5.50 | 98 | 57 | 170 | 194 | 81 | 34 | CMT |
| IV | 33 | 5.19 | 238 | 58 | −6 | 331 | 85 | −148 | CMT |
| IV | 13 | 4.9 | 68 | 72 | −1 | 158 | 89 | −162 | EST |

*CMT; from the Harvard CMT catalog; EST; from this study.

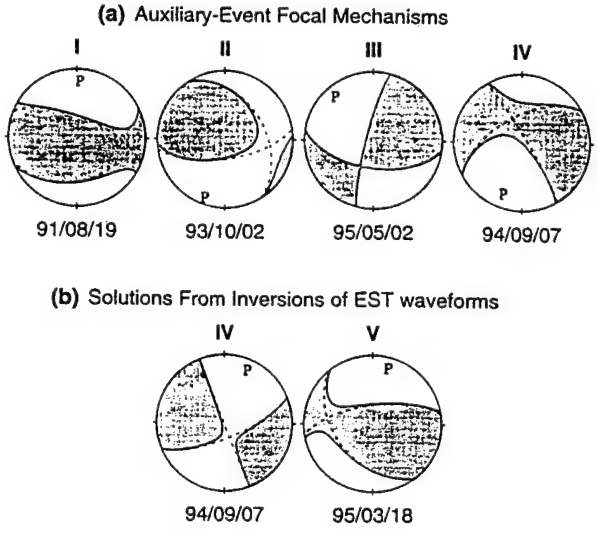


Figure 2. Focal mechanisms for (a) the Harvard CMT solutions for earthquakes listed in Table 2 (dashed lines for best double couples) and (b) moment-tensor solutions obtained in this study (best double couple for event IV: $M_w = 5.2 \pm 0.3$, $\phi = 68 \pm 5°$, $\delta = 72 \pm 10°$, $\lambda = -1 \pm 10°$; event V: $M_w = 4.6 \pm 0.3$, $\phi = 143 \pm 15°$, $\delta = 44 \pm 15°$, $\lambda = 145 \pm 15°$).

able to explore the advantage of the EST algorithm for the characterization of source properties, without detailed modeling of local and regional crustal structure for the Lop Nor area. However, this detailed modeling is critical for constructing adequate deconvolution filters for short-period waves. To this end, various methods of synthetic computations and structure modeling can be utilized (e.g., Herrmann and Wang, 1985; Gomberg and Masters, 1988; Ammon *et al.*, 1990; Saikia, 1994; Gao and Richards, 1994; Herrmann, 1994; Cummins *et al.*, 1994; Geller and Ohminato, 1994; Geller and Takeuchi, 1995).

In the next section, we begin with analysis of the 7 September 1994 earthquake, which is one of the smallest events listed in the Harvard CMT catalog, and discuss in detail the procedure used in this study, in particular, the efforts made for noise-desensitizing deconvolution in calculation of EST waveforms. For other events, we will not repeat detailed discussions on the EST algorithm. For the two underground nuclear explosions, we will focus on the evidence of tectonic release and on the estimation of centroid depths.

## The 7 September 1994 Earthquake

This earthquake occurred in the proximity of the 2 October 1993 earthquake (Fig. 1). The Harvard CMT solution

for the 1994 earthquake was obtained from a data set much smaller than that for the 1993 earthquake: For the 1993 event, the data set includes a total of 90 recordings of long-period body waves (with a cutoff period of 45 sec) at 42 stations and 41 recordings of surface waves (with a cutoff period of 135 sec) at 27 stations; whereas for the 1994 event, it includes only 11 recordings of long-period body waves at eight stations. The standard deviations for the moment-tensor solution listed in the Harvard CMT catalog for the 1994 event are much larger than those for the 1993 event. Since the Harvard CMT solution for the 1993 earthquake is obtained from a large data set with high SNR, including both body and surface waves, we believe that the CMT solution provides an excellent source mechanism for the auxiliary event.

Examination of our data sets for the two earthquakes and for other events used in this study indicates that, in general, for a given station the differences between transverse-component waveforms recorded from various earthquakes are smaller than those for vertical-component and for radial-component waveforms. This may suggest that for our data sets, transverse-component waveforms are less sensitive to differences between source properties or to differences between wave-propagation paths.

Since the 1993 earthquake is much closer in distance to the 1994 earthquake than other earthquakes used in this study, we use the 1993 earthquake as a single auxiliary event. We computed auxiliary-event synthetics using the CMT solution (Table 2 and Fig. 2) and smoothed the data spectra over a frequency window (Press *et al.*, 1986) 1 mHz wide before deconvolution. For data with good SNR, deconvolution with spectral smoothing over a 2-mHz window gives essentially the same results as those for a 1-mHz window.

Various deconvolution methods were used in this study to examine the stability of results obtained from each method. We found that applying the EST algorithm to envelopes of various signals can reduce the amplitude fluctuation of EST waveforms for most stations. We believe that the fluctuation corresponds to large peaks in EST spectra, which result from deconvolution of data spectra with low SNR at various frequencies, where data spectra and synthetic spectra differ significantly in amplitude. Therefore, in the following analysis, we use a procedure to determine separately the instantaneous phase and amplitude (Goodman, 1960) of the EST waveform, which are referred to as the phase transformation and amplitude transformation.

In the amplitude transformation, the algorithm is applied to instantaneous amplitudes of observed and synthetic waveforms. This includes three steps. First, we compute envelopes of observed waveforms for the primary event and envelopes of observed and synthetic waveforms for auxiliary events. Second, we determine the predicted amplitude transfer function for the primary event from observed transfer functions for auxiliary-event envelope spectra using the modified Lagrange interpolation polynomial. Finally, we apply the predicted transfer function to the primary-event envelope spectra, obtaining the EST waveform of the envelope for the primary event.

In the phase transformation, the EST algorithm is applied directly to observed and synthetic waveforms, and the waveform obtained from the transformation is used to calculate the instantaneous phase. Then using the instantaneous phase from the phase transformation and the amplitude from the amplitude transformation, we calculate a time series, which is referred to as the EST waveform with noise desensitization in the following discussions. Our experiments show that the EST-waveform noise-desensitization procedure described above is useful for signals with small SNR, in particular, for records at stations near nodal azimuths of surface-wave radiation patterns.

We use EST waveforms with noise desensitization in analysis of source properties. Figure 3 shows vertical and radial components of displacement records and synthetics at stations HIA and PET along with EST waveforms obtained with and without noise desensitization. The observed waveforms are dominated by high SNR short-period surface waves, arriving much later than in the synthetics. The synthetics for the primary event (1994 earthquake) fit the EST waveforms with noise desensitization much better than for EST waveforms without noise desensitization. For all the events used in this study, variance reductions in inversions of EST waveforms with noise desensitization are much larger than those for EST waveforms without noise desensitization.

To invert the EST waveforms for the moment tensor of the 1994 earthquake, we use the CMT inversion method (Dziewonski *et al.*, 1981; Dziewonski and Woodhouse, 1983). This method involves an iterative procedure to determine the moment tensor as well as centroidal parameters. We show that using EST waveforms enhances the resolution of the location and depth, which is of importance for shallow events with depths less than approximately 35 km in the CMT catalog.

The moment-tensor solution obtained from inversions of EST waveforms (hereafter referred to as the EST solution) has a centroid depth of 13 km, a strike-slip mechanism (Table 2 and Fig. 2), and a centroid location in the proximity of the epicenter reported in PDE. Figure 4 shows vertical and radial components of EST waveforms for the 1994 earthquake for various stations, along with the synthetics computed for the Harvard CMT solution and for the EST solution (hereafter are referred to as the CMT synthetics and EST synthetics, respectively).

The CMT solution has a depth of 33 km, which is the same as the hypocentral depth reported in PDE. In general, for the transverse component, the differences between the CMT synthetics and EST synthetics are much smaller than for the vertical and radial components, reflecting that the transverse component is less sensitive to the variation of source depth or focal mechanisms.

Figure 4 shows that differences between CMT synthetics and EST synthetics become greater at larger epicentral dis-

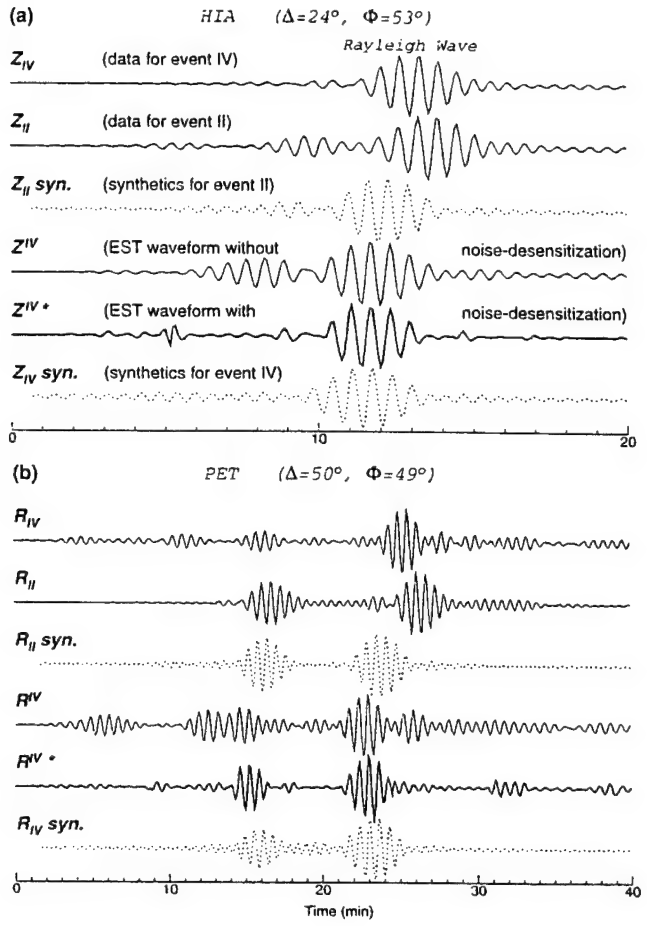


Figure 3. Data and synthetics for stations HIA (Hailar, China) and PET (Petropavlovsk, Russia). Symbols with subscripts indicate vertical ($Z$) and radial ($R$) components of ground displacements for the events listed in Table 1 (subscript identifies the event). Dotted lines indicate synthetics for event II computed using the Harvard CMT solution and for event IV using the moment-tensor solution obtained in this study. EST waveforms for event IV with event II as the auxiliary event are obtained using the EST algorithm without noise desensitization ($Z^{IV}$ and $R^{IV}$) and with noise desensitization ($Z^{IV}$* and $R^{IV}$*). Amplitude is arbitrarily set to show waveform coherence. Time is measured from the origin time of the corresponding event.

tances and that high-mode surface waves are more strongly excited for the CMT synthetics than for the EST synthetics, reflecting the sensitivity of high-mode surface waves to the source depth. While teleseismic waveforms can provide important information on the depth of the source because of better separation of high-mode and fundamental-mode surface waves, for the data set used here, teleseismic waveforms are often not usable because of their small SNR. For example, the radial component at SNZO shows large, abnormal amplitude fluctuations (Fig. 4).

Figure 5 shows data and synthetics for two stations at regional distances from the source. The fit of the synthetics to the EST waveforms is much better than to the observed waveforms, in particular, for station LSA, indicating the utility of EST waveforms for source characterization using regional waveforms. When an appropriate crustal structure model is available, application of the EST algorithm to short-period regional waveforms may provide an important approach for high-resolution analysis of source properties of small earthquakes and explosions.

Figure 6 shows the amplitude ratios between EST waveforms and EST synthetics and between EST waveforms and CMT synthetics. For better comparison, the ratios are shown for all the waveforms available, including waveforms that are not used for the inversions due to their small SNR. It is clear that for all three components, the scatter for the ratios for EST synthetics is smaller than for CMT synthetics.

As discussed earlier, EST waveforms constructed using single auxiliary event depend linearly on the assumed moment tensor of the auxiliary event, and this linear dependence stabilizes primary-event solutions of the centroid depth and location. Several experiments used here indicate that variations of the moment tensor of the EST solution follow approximately a linear relation between the perturbations of the assumed auxiliary-event moment tensor and the derived primary-event moment tensor, as described in (9) and corresponding discussions. For a perturbation of 10% for any components of the auxiliary-event moment tensor, the strike for the best double couple of the EST solution remains about the same, and the variation of the depth for the EST solution is less than 5 km.

## The 18 March 1995 Earthquake

We use this event to examine EST waveforms constructed using multiple auxiliary events, which are listed in Table 2. In the calculation of the synthetics for the 1994 earthquake, we use the EST solution obtained in this study. For other auxiliary events, the synthetics are calculated using the Harvard CMT solutions. We found that the data set for the 18 March 1995 earthquake ($m_b$ = 5.2) clearly has smaller SNR than that for the 7 September 1994 earthquake ($m_b$ = 5.1); this may result from interference with waves from other events near the source area of the 1995 event. However, the EST algorithm still allows us to obtain a centroid depth of 19 ± 5 km, consistent with the depth reported in PDE. The focal mechanism of the moment-tensor solution is shown in Figure 2.

Figure 7a shows the transverse-component waveforms from four auxiliary events recorded at station KMI along with corresponding synthetics. Figure 7b shows the EST waveforms computed using the observed transfer function $\alpha$ for each auxiliary event (hereafter referred to as the single-event EST) and using $\alpha$ obtained by interpolating observed $\alpha$ for the auxiliary events with the modified Lagrange polynomial (hereafter referred to as the multiple-event EST). The interpolation coefficients or weights depend on distances and azimuths of the auxiliary events relative to the primary event. If all the auxiliary events are located at the same depth and in the same distance from the primary event, then the

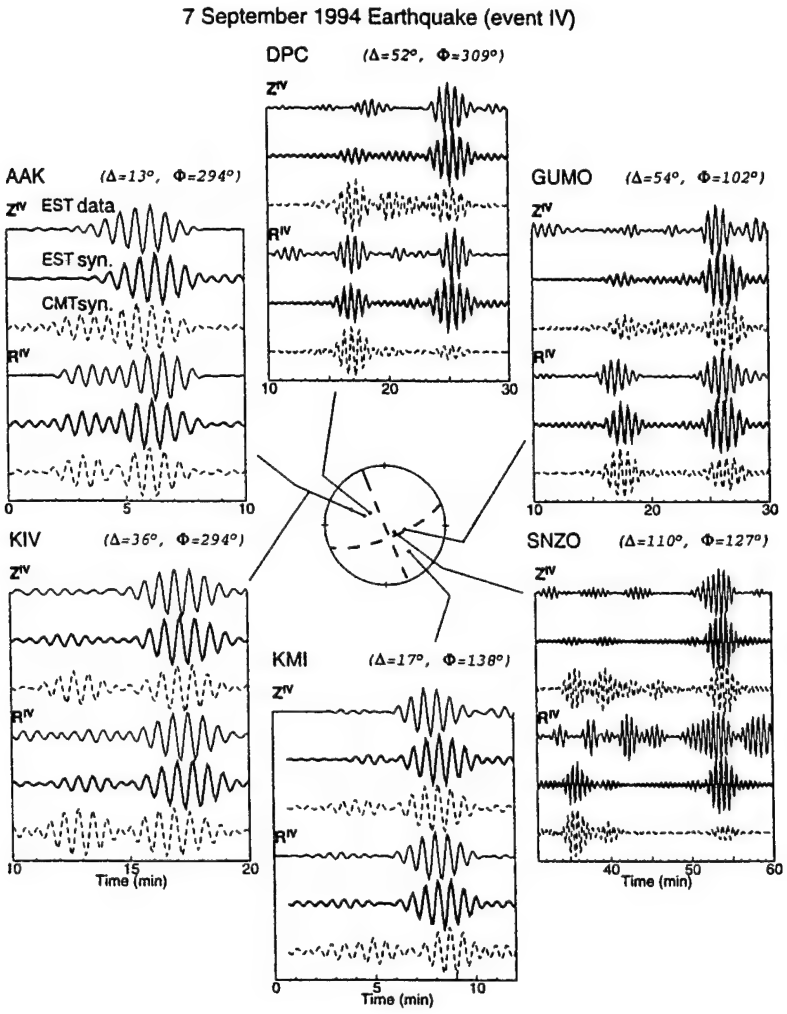


Figure 4. Vertical ($Z^{IV}$) and radial ($R^{IV}$) components of EST waveforms (thin solid lines) and synthetics for the 7 September 1994 earthquake. Thick solid lines show synthetics computed using the EST solution obtained in this study, which has a depth of 13 km. Dashed lines show synthetics computed using the Harvard CMT solution, which has a depth of 33 km. Nodal lines on the focal sphere are for the EST solution.

weight for an auxiliary event is proportional to the sum of the azimuthal angles between the event and its adjacent events relative to the primary event. For the events used here, the weight for event III is about twice as large as those for other auxiliary events, resulting in similar EST waveforms for single-event III $\alpha$ and for multiple-event $\alpha$ (Fig. 7b). Figure 7c shows the multiple-event EST waveform and the synthetic waveform obtained from inversion of multiple-events EST waveforms.

Figure 7d shows the focal mechanism solutions obtained from inversions of single-event EST and multiple-events EST waveforms, demonstrating significant differences between single-event EST solutions. The multiple-events EST solution is similar to the single-event III EST solution, but the multiple-events EST solution has a smaller non-double-couple component.

### The 21 May 1992 and 5 October 1993 Underground Nuclear Explosions

Many studies show that some important features of waveforms from underground nuclear explosions are due to nonisotropic seismic radiation, including the presence of *SH* and Love waves, azimuthal asymmetry of Rayleigh waves, and earthquakelike long-period *P* and *S* waves (e.g., Oliver *et al.*, 1960; Rygg, 1979; Patton, 1980b; Wallace *et al.*, 1983; Herrin and Goforth, 1986; Burger *et al.*, 1986; Wallace, 1991). While it is commonly considered that the nonisotropic seismic radiation was generated by a tectonic-strain release mechanism (Wallace, 1991), the source physics and exact mechanism involved in the tectonic-strain release are not yet well understood.

There are three main hypotheses for the tectonic release mechanism. The first involves explosion-triggered earthquake faulting on nearby faults outside the immediate vicinity of the detonation point (e.g., Brune and Pomeroy, 1963; Aki and Tsai, 1972). Another involves relaxation of deviatoric prestress acting on the source volume, a shattered or explosion-created nonlinear zone surrounding the detonation point (e.g., Archambeau, 1972; Day *et al.*, 1987). And the third involves explosion-driven block motion across rock joints (e.g., Salvado and Minster, 1980). Other secondary sources, such as spall or cavity collapse, were also considered as possible phenomena that affect observed seismic signals from explosions; however, these models have been

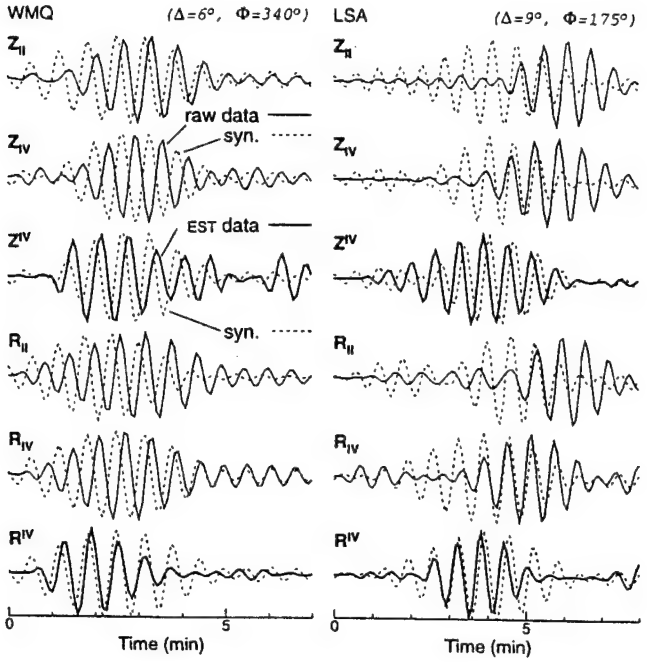


Figure 5. Vertical ($Z$) and radial ($R$) components of displacement waveform data (thin solid lines) for two stations at regional distances from the 7 September 1994 (event IV) and the 2 October 1993 (event II) earthquakes (subscript identifies the event). EST waveforms (thick solid lines) are shown for event IV ($Z^{IV}$ and $R^{IV}$). Synthetics (dashed lines) are computed for event II (auxiliary event) using the Harvard CMT solution and for event IV (primary event) using the EST solution obtained in this study.

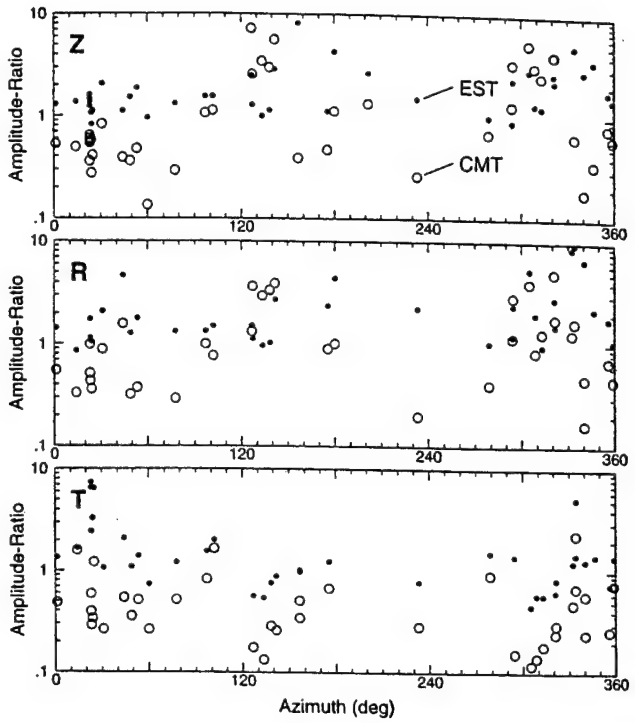


Figure 6. The amplitude ratios between EST waveforms and synthetics plotted on the logarithmic scale for stations at various azimuths from the 7 September 1994 earthquake. The amplitude ratios are calculated for vertical ($Z$), radial ($R$), and transverse ($T$) components, with the synthetics being computed using the EST solution obtained in this study (solid circles) and the Harvard CMT solution (open circles).

found to be inefficient in generating long-period seismic waves with periods 20 sec and longer (Day *et al.*, 1983), although they can be significant sources for higher-frequency waves.

The explosive and tectonic source components are nearly coincident in space and time for the shatter zone model (Day *et al.*, 1987) but may be situated separately for the earthquake-triggering and block-motion models. For the block-motion model, the sense of motion is dominated by thrust-type mechanisms, whereas for the earthquake-triggering model, it is controlled by the regional stress pattern (Wallace, 1991).

The observed seismic signals from the 21 May 1992 and 5 October 1993 underground nuclear explosions at the Lop Nor test site show ample evidences of strong tectonic release: For many stations at $\Delta > 15°$, the amplitude of the transverse component is much larger than for the vertical and radial components, indicating that *SH* and Love waves were more strongly excited than *P-SV* and Rayleigh waves (Figs. 8a and 8b). If an event with the Love/Rayleigh amplitude ratio greater than 0.5 at most stations is ranked, according to Aki and Tsai (1972), as a strong exciter of Love waves, then the two explosions at the Lop Nor test site are clearly very strong Love-wave exciters. Furthermore, the radiation patterns of *P-SV* and Rayleigh waves and of *SH* and Love waves are similar to those for a strike-slip earthquake: There are four lobes for both Rayleigh- and Love-wave radiation patterns, with the lobe directions for the Rayleigh-wave radiation pattern corresponding to the node directions for the Love-wave radiation pattern (Figs. 8a and 8b).

Helle and Rygg (1984) analyzed tectonic release of underground nuclear explosions at the Shagan River test site in eastern Kazakhstan that occurred during 1978 and 1979 using recordings at GDSN stations, which are distributed fairly regularly around the test site and at distances between 1900 and 7150 km. For various explosions, the largest Love/Rayleigh (transverse/vertical) amplitude ratio amounts to about 2.5, which is observed for an explosion with strongest tectonic release. However, this amplitude ratio is smaller than those for many stations for the 21 May 1992 explosion, as shown in Figure 8a.

Figure 8c shows the displacement waveforms for the 2 May 1995 earthquake, which has a strike-slip mechanism and a depth of 18 km (Table 2 and Figs. 1 and 2); its recordings are dominated by *SH*- and Love-wave energy, except for stations CHTO and KIP, which are located at azimuths differing significantly from the strikes of the nodal planes for the focal mechanism of the earthquake. With the

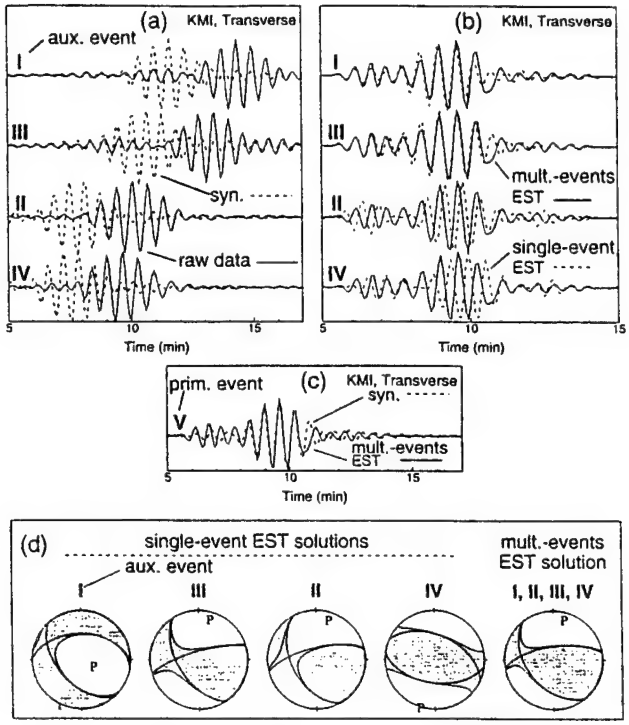


Figure 7. (a) Transverse-component displacement waveforms (solid lines) recorded at station KMI (25° in distance and 103° in azimuth from the 18 March 1995 earthquake) from various auxiliary events along with synthetics (dashed lines) computed using the Harvard CMT solutions for events I, II, and III and the EST solution for event IV. (b) Solid lines show the multiple-events EST waveform obtained using $\alpha$ that is calculated by interpolating observed $\alpha$ for various auxiliary events; dashed lines show single-event EST waveforms obtained using observed $\alpha$ for each auxiliary event. (c) The multiple-events EST waveform (solid line) and synthetic waveform (dashed line) computed using the solution obtained from inversion of multiple-events EST waveforms. (d) Focal mechanism solutions obtained from inversions of single-event EST waveforms for each auxiliary event and from inversion of multiple-events EST waveforms.

exception of station CHTO, for all the stations shown in Figure 8, the amplitude ratios of the vertical component to the radial component and to the transverse component for the 1992 explosion are about the same as those for the 1993 explosion, implying that seismic waves from these explosions have similar radiation patterns. In the following, we examine in detail the observed waveforms shown in Figure 8a for the 21 May 1992 explosion.

It is well known that *SH*- and Love-wave energy on seismic signals from underground explosions is caused only by tectonic release. The Rayleigh-wave energy, however, is due to the combined effects of the explosive source and the tectonic release. For long-period waves used in this study, the nonisotropic radiation of the tectonic release for stations on radiation pattern lobes appears to be much stronger than the isotropic radiation of the explosive source. Note that for the 1992 explosion, the amplitudes of Rayleigh waves on vertical and radial components at station KIP are approximately four times larger than those for station CTAO (Fig. 8a), implying that Rayleigh waves excited by the tectonic release for stations on radiation pattern lobes are much larger than those excited by the explosive source, which are azimuthly independent.

Figure 8a shows that there are large differences between amplitudes of various components for stations AAK, GAR, and KIV: The amplitudes of vertical and radial components are about the same as those of the transverse component for stations AAK and GAR, but they are much smaller than that of the transverse component for station KIV. Note that all the stations are located at similar azimuths from the source, which are 280°, 266°, and 290°, for AAK, GAR, and KIV, respectively; however, AAK and GAR are located at regional distances, while KIV is located at teleseismic distance.

The differences between amplitudes of various components described above may be attributed, in part, to the effects of high-mode surface waves. It is well known that high-mode surface-wave energy is more prominent on regional seismograms than on teleseismic ones and that it involves a superposition of many high-mode waves with different radiation patterns. Therefore, for tectonic release, the radiation of high-mode surface waves is more isotropic than that of fundamental-mode surface waves, resulting in reduced azimuthal variations of amplitudes among stations at regional distances (i.e., AAK and GAR) in comparison with more pronounced anisotropic radiation at low frequencies. For KIV, the fundamental-mode surface-wave energy becomes dominant, and for tectonic release, its radiation is anisotropic, with the amplitude depending on the station azimuth from the source for a given epicentral distance.

With the exception of stations at regional distances, namely, AAK and GAR, the observed waveforms for the 1992 explosion clearly show radiation patterns similar to those for a strike-slip earthquake (Fig. 8a). For stations located at azimuths close to the two orthogonal directions of azimuths 20°/200° and 110°/290° (i.e., OBN, KIV, GUMO, COL, TOL, CTAO, COR, CCM, and PAS), *P-SV* and Rayleigh waves are small in amplitude relative to stations at similar distances from the source, while *SH* and Love waves are large. In contrast, for stations at azimuths differing significantly from these directions (i.e., CHTO, KEV, NWAO, and KIP), *P-SV* and Rayleigh waves are large, while *SH* and Love waves are small.

The presence of earthquakelike radiation patterns of *P-SV* and Rayleigh waves and of *SH* and Love waves for stations at teleseismic distances suggests that the two underground nuclear explosions at the Lop Nor test site caused or triggered significant tectonic release of a strike-slip mechanism, with the nodal planes being subparallel to those of the 2 May 1995 earthquake, which was located northwest of the test site near a major active fault in the Tien Shan mountains (Fig. 1).

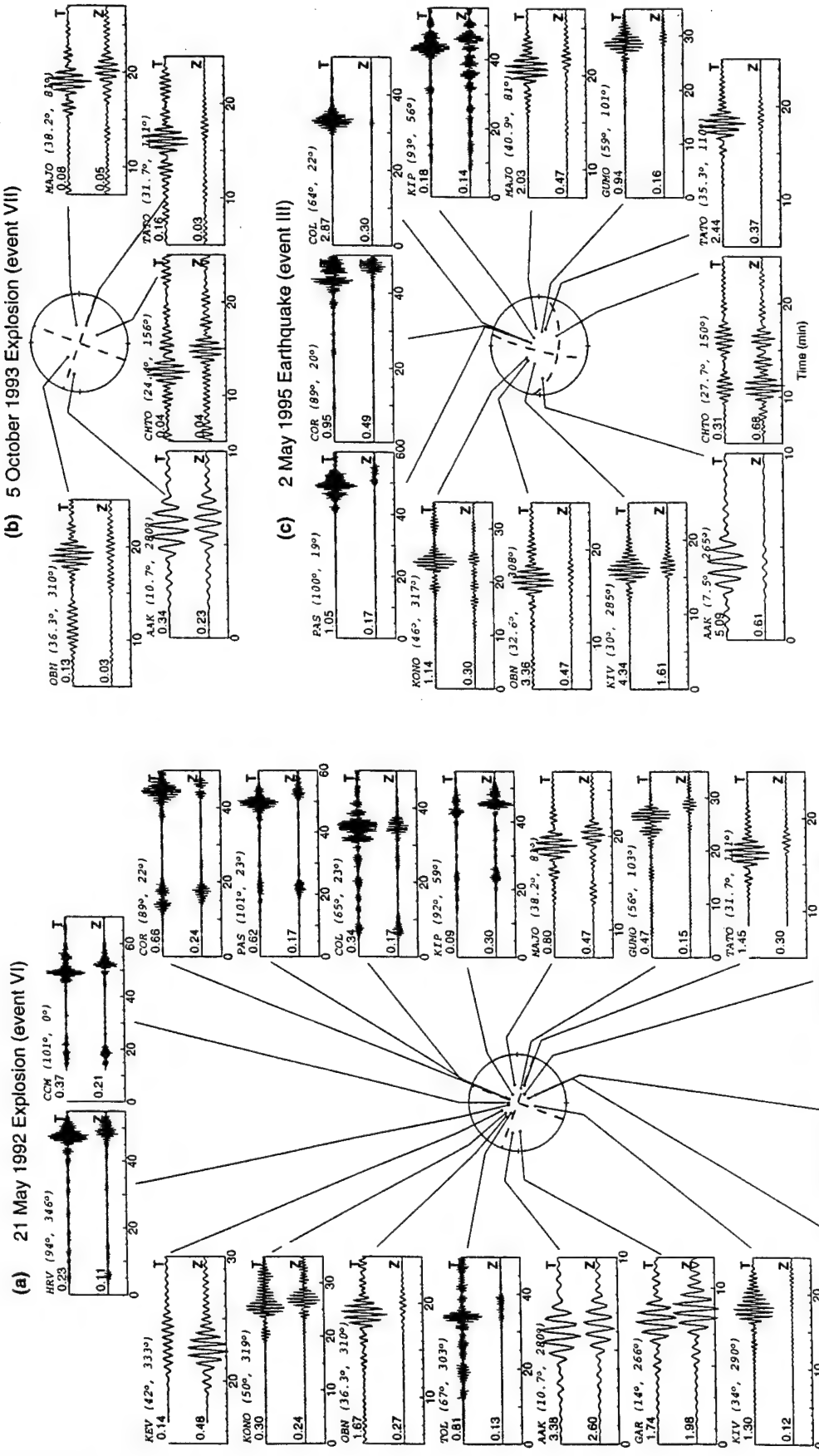


Figure 8. Vertical ($Z$) and transverse ($T$) components of displacement waveforms recorded at various stations from (a) the 21 May 1992 and (b) the 5 October 1993 underground nuclear explosions, and from (c) the 2 May 1995 earthquake. The number shown above each waveform indicates amplitude in the unit of microns. For each station event pair, all the components are plotted on the same scale; numbers in parentheses indicate the distance and azimuth of the station from the source. Bandpass filter with corner frequencies 20 and 30 mHz applied. Nodal lines on the focal sphere for the explosions are for an assumed strike-slip mechanism (strike 20°, dip 90°, slip 0°) and for the earthquake are for the CMT solution.

Using the formula of Jih and Wagner (1991), Li *et al.* (1995) estimated the depths of burial for the 21 May 1992 and 5 October 1993 explosions to be 0.71 and 0.46 km, respectively. These depths are much shallower than the depths of all the earthquakes studied here (Tables 1 and 2). To explore the potential of using the EST algorithm to characterize the source of these explosions including tectonic release, we carried out two experiments. Recognizing the difficulty in separating the effects of the explosive source at the burial depth and the effects of any anisotropic sources at other depths, we use a point-source approximation to the complete centroid moment tensor, which includes both the explosion part (isotropic) and the tectonic release part (non-isotropic), to characterize the combined seismic radiation of the explosion plus tectonic release.

In the first experiment, we obtained EST waveforms for the 1992 and the 1993 explosions using the earthquakes listed in Table 2 as the auxiliary events. For each explosion, inversions of the EST waveforms yielded a shallow centroid depth (<10 km) for the combined source of explosion and tectonic release; however, the results of inversions showed strong data dependency. This may reflect limited resolution of the EST algorithm, which is due, in part, to the fact that the chosen auxiliary events are situated at depths much deeper than that of the primary event (underground nuclear explosion). Note that all the auxiliary events used here have depths deeper than 10 km (Table 2), while the depths of the explosive sources are shallower than 1 km, and the depths of tectonic release for these explosions may be much shallower than 10 km.

To improve source characterization of underground nuclear explosions plus tectonic release, a possible approach is to include one of the explosions in the auxiliary event set and invert for the other explosion, or to use a shallow earthquake located at the test site with depth shallower than, say, 10 km as the auxiliary event. This step requires that the depth of the auxiliary event is independently determined, which involves efforts beyond the scope of this study.

In the second experiment, we utilize the linear dependence of EST waveforms on the auxiliary-event moment tensor, as shown in equation (9) and corresponding descriptions in the previous section, to estimate the range of possible centroid depth of the 5 October 1993 explosion plus tectonic release, with the 21 May 1992 explosion being taken as the auxiliary event. For a data set with each record being dominated by a single-pathing wave packet, the linear dependence allows us to estimate the depth and location of the primary event, without knowing the correct focal mechanism of the auxiliary event.

In this experiment, we use various trial depths and an assumed moment tensor in calculation of synthetics for the auxiliary event, the 21 May 1992 explosion. For simplicity, all the elements of the moment tensor are assumed to be unity. Additional experiments conducted in this study confirm that any variation of the assumed moment tensor of the auxiliary event does not affect the centroid depth estimate of the primary event, the 5 October 1993 explosion plus tectonic release.

Figure 9 shows the results from the second experiment, including the centroid depth estimates of the 1993 explosion plus tectonic release and variance reductions of inversions. For various assumed depths of the auxiliary event of 10 km or less, the centroid depth of the 1993 explosion plus tectonic release is estimated at approximately 4 km. The maximum variance reduction was obtained at 10-km depth of the auxiliary event; however, the relation between variance reductions and assumed auxiliary-event depths appears to be unsystematic, so we do not consider that the centroid depth of the 21 May 1992 explosion plus tectonic release (auxiliary event) is resolved in this experiment. This unsystematic variance reduction reflects the limited resolution of the passband used in this study.

Our estimate of the centroid depth of the 5 October 1993 explosion plus tectonic release is about 4 km, which is much deeper than the 0.46-km burial depth of the explosion estimated by Li *et al.* (1995). Given the presence of large *SH* and Love waves and the strike-slip type of radiation patterns of Rayleigh and Love waves, the difference between the burial and centroid depths suggests that large tectonic release was caused by the explosion and occurred at depths deeper than the depth of the explosive source, with released tectonic strains being associated with major active faults in the vicinity of the Lop Nor test site (Fig. 1). Several recent earthquakes, which occurred within 1-km epicentral distance

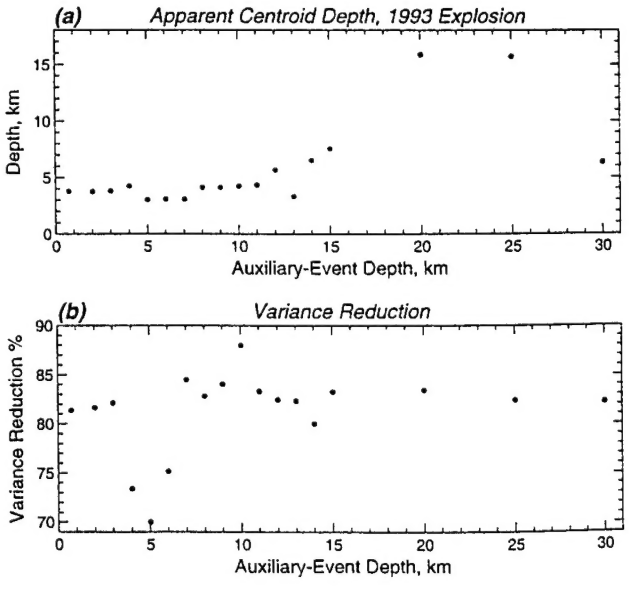


Figure 9. (a) Apparent depth of the centroid of the 5 October 1993 explosion plus tectonic release obtained from inversions of EST waveforms, which are calculated using the 21 May 1992 explosion as the auxiliary event. Abscissas indicate assumed centroid depths of the auxiliary event in calculation of EST waveforms. (b) Maximum variance reduction in iterative inversions of EST waveforms.

from some underground nuclear explosions, have depths of about 10 km and $m_b$ about 4, as reported in PDE, indicating seismic strain release at deeper depths under the test site.

## Discussion

Despite the difficulty in the determination of "epicentral depth" for tectonic release, several investigations suggest that the explosive and tectonic-release sources were not coincident in space as assumed in the shatter zone model of Day *et al.* (1987). For Pahute-Mesa explosions, all the explosive-source depths are less than 1 km; however, using the relative timing between the onset of the explosion *P* wave and *sP* at upper mantle distances, Wallace (1991) estimated the centroid depths of the largest explosions at between 2 and 4 km, and the radius of the volume that produces seismic waves at approximately 2 to 4 times the depth of burial.

For a Pahute-Mesa explosion with high-tectonic release, Burger *et al.* (1986) estimated the moment for tectonic release at about twice as large as for the explosion. In modeling teleseismic, long-period *P* and *S* waves from some southern and northern Novaya Zemlya explosions, Burger *et al.* (1986) used one source at a depth of 2 km with a strike-slip or 45°-dipping fault mechanism and another at a depth of 3 km with an oblique-normal fault mechanism.

As reported in many investigations of seismic radiation from underground nuclear explosions, there is ample evidence of tectonic release on surface waves and long-period body waves; however, the evidence of tectonic release on short-period body waves ($f > 0.5$ Hz) is relatively rare. An interesting example for the evidence on short-period energy is the 1988 Soviet Joint Verification Experiment, underground nuclear explosion. In analysis of broadband data from the explosion, Langston (1995) found that the "tectonic release" is composed of two parts: the first is attributed to cavity relaxation, which dominates at long periods ($f < 0.3$ Hz), and the second is inferred to be caused by explosion-driven block motions with no net moment, which is located 2 to 3 km south of the shot point. The second source is seen from *SH* data, which show a large, unexpected, high-frequency ($f > 1$ Hz) arrival after *SmS*.

The Soviet JVE explosion is not considered to have a significantly large tectonic release component at long periods (Sykes and Ekström, 1989). This explosion was well recorded at two stations located from the JVE at azimuths differing by about 40° and at approximately the same distances (255 km). For both stations, the amplitudes of long-period ($f < 0.3$ Hz) *SH* and Love waves are approximately 2 to 4 times smaller than for *P-SV* and Rayleigh waves (Priestley *et al.*, 1990; Walter and Patton, 1990; Langston, 1995). The small *SH*- and Love-wave generation is in clear contrasts with recordings from the 21 May 1992 and 5 October 1993 underground nuclear explosions at the Lop Nor test site, which show that amplitudes of *SH* and Love waves are much larger than for *P-SV* and Rayleigh waves for many stations (Fig. 8).

For underground nuclear explosions, a critical problem in understanding the relation between the explosive source and tectonic release is how to separate the effects of the two types of source. This problem may be solved in part by applying the EST algorithm to transverse-component waveforms alone to determine the centroid parameters of tectonic release, since *SH* and Love waves are caused only by tectonic release and not directly affected by the explosive source. Given the depth sensitivity of short-period waves, for optimal determination of tectonic release, it is desirable to use short-period *SH* and Love waves in our future application of the EST algorithm, extending earlier studies directed at modeling short-period regional waves with adequate crustal structure models (e.g., Helmberger and Malone, 1975; Langston, 1981, 1994; Bent *et al.*, 1989; Dreger and Helmberger, 1991; Fan and Wallace, 1991; Helmberger *et al.*, 1992; Herrmann, 1994; Zhao and Helmberger, 1994).

Implicit in the EST algorithm used here is the assumption that transfer function $\alpha$ is independent of the calibration-event source focal mechanism. However, for short-period waves in strong laterally varying structure, which is the primary use of empirical calibrations in seismic-event monitoring, interference may occur between multipathing waves with different propagation characteristics, which prevents partitioning data into records using time- or frequency-filtering techniques with each record containing a dominant single-pathing wave train.

Therefore, it is necessary to define the transfer function ($\alpha$) as a tensor and estimate it using multiple calibration events, with each component of the $\alpha$ tensor corresponding to an excitation coefficient or Green's function in (1). The differences between various components of the $\alpha$ tensor represent the effects of the complexity of the actual Earth's structure, including multipathing, which are not predicted by a given simple Earth model. Then the location, depth, and source properties of small seismic events can be determined using the excitation coefficients or Green's functions that are modified using corresponding components of the $\alpha$ tensor. Note that when all the components of $\alpha$ are identical, modifying excitation coefficients is equivalent to simplifying observed waveforms, and the $\alpha$ tensor can be represented by a scalar quantity, which is the approximation used in the EST algorithm presented in this study.

## Conclusions

In this study, we present an approach to estimating seismic source parameters when the velocity structure is only moderately constrained. The approach is to remove the effect of an idealized, reference Earth's structure from the data by deconvolving a set of calibration events with Green's functions for the reference structure, with the remaining signal being the transfer function between the actual structure and the assumed ideal structure assuming that the source of the calibration events is precisely known. These transfer func-

tions ($\alpha$) are then deconvolved from the target event producing simplified waveforms that are then inverted using the idealized Green's functions.

Several experiments were carried out to test the (EST) algorithm in the determination of the source mechanism and centroid time, location, and depth of earthquakes and nuclear explosions in Xinjiang, China. The algorithm allows us to use GSN data and the standard Earth model (PREM) to obtain improved resolution of source characterization for earthquakes with $m_b$ about 5 in the Lop Nor area, without detailed modeling of local and regional structure.

For the 7 September 1994 earthquake ($m_b$ = 5.1), we obtained a depth of 13 km, which is significantly shallower than the 33-km depth reported in PDE and in the Harvard CMT catalog. For the 18 March 1995 earthquake ($m_b$ = 5.2), we obtained a depth of about 19 km, consistent with that reported in PDE. For the EST algorithm, which involves only one auxiliary event and data sets with each record dominated by a single-pathing wave train, the centroidal parameters (time, location, and depth) of the primary event obtained from inversions of EST waveforms are insensitive to the assumed source mechanism of the auxiliary event used in construction of the deconvolution filter. This allows us to determine the apparent depth of the 5 October 1993 nuclear explosion plus tectonic release by using the 21 May 1992 explosion as the auxiliary event.

Our analysis suggests that the centroid depth of the 5 October 1993 nuclear explosion plus tectonic release is about 4 km and that of the 21 May 1992 explosion plus tectonic release is not well resolved and may be deeper than 5 km, reflecting limited resolution of the passband used in this study. With extension to shorter-period energy, the method holds promise for reliable source inversion for small events in a calibrated region.

## Acknowledgments

The author is grateful for helpful comments on the manuscript from Anton M. Dainty, Thorne Lay, Lian-She Zhao, and the anonymous reviewer and discussions with Thorne Lay and Howard Patton on the tectonic release in underground nuclear explosions. The data used in this study were made available by courtesy of the IRIS/DMC. This work was supported by AFOSR Grant F49620-94-1-0315. Contribution Number 310 of the W. M. Keck Seismological Laboratory and the Institute of Tectonics, University of California, Santa Cruz.

## References

Aki, K. and Y. B. Tsai (1972). Mechanism of Love wave excitation by explosion sources, *J. Geophys. Res.* **77,** 1452–1475.

Ammon, C. J., G. E. Randall, and G. Zandt (1990). On the non-uniqueness of receiver function inversions, *J. Geophys. Res.* **95,** 15303–15318.

Archambeau, C. B. (1972). The theory of stress wave radiation from explosions in prestressed media, *Geophys. J.* **29,** 329–366.

Bent, A. L., D. V. Helmberger, R. J. Stead, and P. Ho-Liu (1989). Waveform modeling of the November 1987 Superstition Hills earthquakes, *Bull. Seism. Soc. Am.* **79,** 500–514.

Brune, J. N. and P. N. Pomeroy (1963). Surface wave radiation patterns for underground nuclear explosions and small-magnitude earthquakes, *J. Geophys. Res.* **68,** 5005–5028.

Burger, R. W., T. Lay, T. C. Wallace, and L. J. Burdick (1986). Evidence of tectonic release in long-period S waves from underground nuclear explosions at the Novaya Zemlya test sites, *Bull. Seism. Soc. Am.* **76,** 733–755.

Cummins, P. R., R. J. Geller, and N. Takeuchi (1994). Complete seismic wavefield calculations for strong upper mantle heterogeneity, *EOS* **75,** 422.

Dahlquist, G. and Å. Björck (1974). *Numerical Methods,* Prentice-Hall, Englewood Cliffs, New Jersey, 284–285.

Day, S. M., N. Rimer, and J. T. Cherry (1983). Surface waves from underground explosions with spall: analysis of elastic and nonlinear source models, *Bull. Seism. Soc. Am.* **73,** 247–264.

Day, S. M., J. T. Cherry, N. Rimer, and J. L. Stevens (1987). Nonlinear model of tectonic release from underground explosions, *Bull. Seism. Soc. Am.* **77,** 996–1016.

Dreger, D. S. and D. V. Helmberger (1991). Complex faulting deduced from broadband modeling of the 28 February 1990 Upland earthquake ($M_L$ = 5.2), *Bull. Seism. Soc. Am.* **81,** 1129–1144.

Dziewonski, A. M. and D. L. Anderson (1981). Preliminary reference Earth model, *Phys. Earth Planet. Interior* **25,** 297–356.

Dziewonski, A. M. and J. H. Woodhouse (1983). An experiment in systematic study of global seismicity: centroid-moment tensor solutions for 201 moderate and large earthquakes of 1981, *J. Geophys. Res.* **88,** 3247–3271.

Dziewonski, A. M., T.-A. Chou, and J. H. Woodhouse (1981). Determination of earthquake source parameters from waveform data for studies of global and regional seismicity, *J. Geophys. Res.* **86,** 2825–2852.

Fan, G. and T. C. Wallace (1991). The determination of source parameters for small earthquakes from a single, very broadband seismic station, *Geophys. Res. Lett.* **18,** 1385–1388.

Gao, L. and P. G. Richards (1994). Studies of earthquakes on and near the Lop Nor, China, nuclear test site, *Proc. of the 16th Annual Seismic Research Symposium,* Phillips Laboratory, Hanscom AFB, MA, 106–112.

Geller, R. J. and T. Ohminato (1994). Computation of synthetic seismograms and their partial derivatives from heterogeneous media with arbitrary natural boundary conditions using the direct solution method, *Geophys. J. Int.* **116,** 421–446.

Geller, R. J. and N. Takeuchi (1995). A new method for computing highly accurate DSM synthetic seismograms, *Geophys. J. Int.* **123,** 449–470.

Gilbert, F. and A. M. Dziewonski (1975). An application of normal mode theory to the retrieval of structure parameters and source mechanisms from seismic spectra, *Philos. Trans. Roy. Soc. London A* **278,** 187–269.

Gomberg, J. S. and T. G. Masters (1988). Waveform modeling using locked-mode synthetic and differential seismograms: application to determination of the structure of Mexico, *Geophys. J.* **94,** 193–218.

Goodman, N. R. (1960). Measuring amplitude and phase, *J. Franklin Inst.* **270,** 437–450.

Helle, H. B. and E. Rygg (1984). Determination of tectonic release from surface waves generated by nuclear explosions in eastern Kazakhstan, *Bull. Seism. Soc. Am.* **74,** 1883–1898.

Helmberger, D. V. and D. G. Harkrider (1973). Seismic source descriptions of underground explosions and a depth discriminate, *Geophys. J. R. Astr. Soc.* **31,** 45–63.

Helmberger, D. V. and S. D. Malone (1975). Modeling local earthquakes as shear dislocations in a layered half space, *J. Geophys. Res.* **80,** 4881–4888.

Helmberger, D. V., R. Stead, P. Ho-Liu, and D. Dreger (1992). Broadband modeling of regional seismograms: Imperial Valley to Pasadena, *Geophys. J. Int.* **110,** 42–54.

Herrin, E. and T. Goforth (1986). Phase analysis of Rayleigh waves from the Shagan River test site in the USSR, *Bull. Seism. Soc. Am.* **76,** 1739–1754.

Herrmann, R. B. (1994). Waveform inversion of broadband regional seismograms, *Seism. Res. Lett.* **65,** 28.

Herrmann, R. B. and C. Y. Wang (1985). A comparison of synthetic seismograms, *Bull. Seism. Soc. Am.* **75,** 41–56.

Hu, F., J. Hu, M. Bai, S. Chen, D. Zhou, and J. Liu (1989). Seismotectonics of Xinjiang Uygur Autonomous Region, in *Lithospheric Dynamics Atlas of China*, Editorial Board for Lithospheric Dynamics Atlas of China, State Seismological Bureau, China Cartographic Publishing House, Beijing, 57.

Jih, R.-S. and R. A. Wagner (1991). Recent methodological developments in magnitude determination and yield estimation with applications to Semipalatinsk explosions, *Tech. Rep. PL-TR-91-2212 (I)*, Phillips Laboratory, Hanscom, 90.

Langston, C. A. (1981). Source inversion of seismic waveforms; the Koyna, India, earthquakes of 13 September 1967, *Bull. Seism. Soc. Am.* **71**, 1–24.

Langston, C. A. (1994). An integrated study of crustal structure and regional wave propagation for southeastern Missouri, *Bull. Seism. Soc. Am.* **84**, 105–118.

Langston, C. A. (1995). Anatomy of regional phases and source characterization of the Soviet joint verification experiment, underground nuclear explosion, *Bull. Seism. Soc. Am.* **85**, 1416–1431.

Lay, T., D. V. Helmberger, and D. G. Harkrider (1984). Source models and yield-scaling relations for underground nuclear explosions at Amchitka Island, *Bull. Seism. Soc. Am.* **73**, 843–862.

Li, Y., M. N. Toksöz, and W. Rodi (1995). Source time functions of nuclear explosions and earthquakes in central Asia determined using empirical Green's functions, *J. Geophys. Res.* **100**, 659–674.

Matzko, J. R. (1992). Geology of the Chinese nuclear test site near Lop Nor, Xinjiang province, China, *Proc. of the 14th Annual PL/DARPA Seismic Research Symposium*, Phillips Laboratory, Hanscom, 197–303.

Matzko, J. R. (1994). Geology of the Chinese nuclear test sites near Lop Nor, Xinjiang Uygur Autonomous Region, China, *Eng. Geol.* **36**, 173–181.

Murphy, J. R. (1995). An overview of seismic discrimination issues relevant to CTBT monitoring, presented at *The 17th Annual Seismic Research Symposium on CTBT Monitoring*, Phillips Laboratory, Hanscom, 3–4.

Murphy, J. R. and R. A. Mueller (1971). Seismic characteristics of underground nuclear detonations; Part II, Elastic energy and magnitude determinations, *Bull. Seism. Soc. Am.* **61**, 1693–1704.

Oliver, J., P. Pomeroy, and M. Ewing (1960). Long-period surface waves from nuclear explosions in various environments, *Science* **131**, 1804–1805.

Patton, H. J. (1980a). Reference point equalization method for determining the source and path effects of surface waves, *J. Geophys. Res.* **85**, 821–848.

Patton, H. J. (1980b). Surface-wave generation by underground nuclear explosions releasing tectonic strain, Lawrence Livermore Laboratory Report UCRL-53062, Livermore, California.

Patton, H. J. (1991). Seismic moment estimation and the scaling of the long-period explosion source spectrum, in *Explosion Source Phenomenology*, S. R. Taylor, H. J. Patton, and P. G. Richards (Editors), Geophysical Monograph 65, American Geophysical Union, Washington, D.C., 171–183.

Press, W. H., B. P. Flannery, S. A. Teukolsky, and W. T. Vetterling (1986). *Numerical Recipes: The Arc of Scientific Computing*, Cambridge Univ. Press, Cambridge, 495.

Priestley, K. F., W. R. Walter, V. Martynov, and M. V. Rozhkov (1990). Regional seismic recordings of the Soviet nuclear explosion of the Joint Verification Experiment, *Geophys. Res. Lett.* **17**, 179–182.

Rygg, E. (1979). Anomalous surface waves from underground nuclear explosions, *Bull. Seism. Soc. Am.* **69**, 1995–2002.

Saikia, C. K. (1994). Modified frequency-wavenumber algorithm for regional seismograms using Filon's quadrature-modeling of Lg waves in North America, *Geophys. J. Int.* **118**, 142–158.

Salvado, C. and J. B. Minster (1980). Slipping interfaces: a possible source of S radiation from explosive sources, *Bull. Seism. Soc. Am.* **70**, 659–670.

Sykes, L. and G. Ekström (1989). Comparison of seismic and hydrodynamic yield determinations for the Soviet joint verification experiment of 1988, *Proc. Natl. Acad. Sci. USA* **86**, 3456–3460.

Toksöz, M. N., A. Ben-Menahem, and D. G. Harkrider (1964). Determination of source parameters of explosions and earthquakes by amplitude equalization of seismic surface waves, Part 1, Underground nuclear explosions, *J. Geophys. Res.* **69**, 4355–4366.

Wallace, T. C. (1991). Body wave observations of tectonic release, in *Explosion Source Phenomenology*, S. R. Taylor, H. J. Patton, and P. G. Richards (Editors), Geophysical Monograph 65, American Geophysical Union, Washington, D.C., 161–170.

Wallace, T. C., D. V. Helmberger, and G. R. Engen (1983). Evidence of tectonic release from underground nuclear explosions in long-period P waves, *Bull. Seism. Soc. Am.* **73**, 593–613.

Wallace, T. C., D. V. Helmberger, and G. R. Engen (1985). Evidence of tectonic release from underground nuclear explosions in long-period S waves, *Bull. Seism. Soc. Am.* **75**, 157–174.

Walter, W. R. and H. J. Patton (1990). Tectonic release from the Soviet Joint Verification Experiment, *Geophys. Res. Lett.* **17**, 1517–1520.

Weidner, D. J. and K. Aki (1973). Focal depth and mechanism of mid-ocean ridge earthquakes, *J. Geophys. Res.* **78**, 1818–1831.

Wu, F. T. and A. Levshin (1994). Surface-wave group velocity tomography of East Asia, *Phys. Earth Planet. Interior* **84**, 59–77.

Zhao, L.-S. and D. V. Helmberger (1994). Source estimation from broadband regional seismograms, *Bull. Seism. Soc. Am.* **84**, 91–104.

Institute of Tectonics
University of California
Santa Cruz, California 95064

Manuscript received 4 September 1996.